

RSC Advances



This is an *Accepted Manuscript*, which has been through the Royal Society of Chemistry peer review process and has been accepted for publication.

Accepted Manuscripts are published online shortly after acceptance, before technical editing, formatting and proof reading. Using this free service, authors can make their results available to the community, in citable form, before we publish the edited article. This *Accepted Manuscript* will be replaced by the edited, formatted and paginated article as soon as this is available.

You can find more information about *Accepted Manuscripts* in the [Information for Authors](#).

Please note that technical editing may introduce minor changes to the text and/or graphics, which may alter content. The journal's standard [Terms & Conditions](#) and the [Ethical guidelines](#) still apply. In no event shall the Royal Society of Chemistry be held responsible for any errors or omissions in this *Accepted Manuscript* or any consequences arising from the use of any information it contains.

Title: Conducting Poly (o-anisidine-co-o-phenyldiammine) nanorods dispersed epoxy composite coatings: Synthesis, characterization and corrosion protective performance

Names of Authors

Neha Kanwar Rawat

Research scholar

Materials Research Laboratory, Dept of Chemistry

Jamia Millia Islamia, New Delhi. 110025.

Email: neharawatjmi@gmail.com

Dr. Alok Kumar Sinha

Scientist E

Department of Science and Technology

New Delhi

Email: alokkumar.sinha@nic.in

*Prof. Sharif Ahmad

Materials Research Laboratory, Dept of Chemistry

Jamia Millia Islamia, New Delhi. 110025.

Email: sharifahmad_jmi@yahoo.co.in

***Corresponding Author**

Tel no. +91 11 26827508

Fax: +91 11 26840229

Conducting Poly (o-anisidine-co-o-phenyldiammine) nanorods dispersed epoxy composite coatings: Synthesis, characterization and corrosion protective performance

Neha Kanwar Rawat¹, Alok Kumar Sinha² and Sharif Ahmad*¹

(1) Materials Research Laboratory, Department of Chemistry, Jamia Millia Islamia, New Delhi-110025, India

(2) Department of Science and Technology (DST), New Delhi, India

Abstract: Conducting polymers (CPs) have been significantly contributing to the development of high performance new-generation anti-corrosive coatings. CPs nanofiller dispersed insulating polymer coating effectively prevents the transport of corrosive ions (H^+ , O^{2-} , Cl^- , OH^- etc) at coating-metal interface, via barrier or redox mechanism. In view of this, for the first time, we report the synthesis of poly (o-anisidine-co-o-phenyldiammine) P(oA-co-oPDA) copolymer conducting nanorods. Poly (o-anisidine) (PoA) conducting nanoparticles were also synthesized laterally. The formulation of these nanofillers dispersed epoxy-polyamide (PA) nanocomposite coating systems have also been reported. The structural elucidation was performed by FT-IR, UV-Vis, 1H NMR spectroscopy. The crystallinity, surface area and morphology of fillers were analysed by XRD, BET, SEM and TEM techniques. The thermal stability and hydrophobic behaviour were investigated using TGA, DSC and contact angle measurements. The physico-mechanical properties and corrosion protective performance of these coatings were evaluated using standard methods. The salt spray test, potentiodynamic polarization (PDP) and electron impedance spectroscopy studies (EIS) were conducted in 5 wt % NaCl and 5 wt % HCl media. The physico-mechanical properties, corrosion protection performance and Raman studies

revealed that the P(oA-co-oPDA)-epoxy-PA nanocomposite coating have exhibited superior performance than those of PoA-epoxy-PA, epoxy-PA and other such nanocomposite coatings.

*Corresponding author: E-mail: sharifahmad_jmi@yahoo.co.in Tel: +91 11 26827508. Fax: +91 11 26840

Keywords: P (o-anisidine), conducting nanorods, copolymerization, hydrophobicity, corrosion protection

1. INTRODUCTION

Corrosion of structural materials is considered to be a serious problem for industries and impads the economy of the country. Generally, three approaches are being used to reduce such undesirable natural process causing huge losses to the metallic materials via-a-vis (i) cathodic protection ¹ (ii) anodic protection (passivation) ² and (iii) application of barrier coatings ³. Further significant progress has been made in the designing of nano CP coatings. Thus, the focus of scientific research has shifted towards the development of a new generation of smart CP based protective coating materials, possessing high wear and corrosion resistance ability³.

Conducting polymers such as PANI, PPy and PTh seems to be interesting materials that find application in the field of fundamental research pertaining to engineering and technology ⁴. Among them PANI and their derivatives are considered to be the most promising materials because of their ease of synthesis, non-toxic, high electrical conductivity, chemical stability, redox reversibility and low cost. These polymers due to their excellent anti-corrosive ability and environmental stability have attracted considerable attention in the field of corrosion inhibition and protective coatings. However, their poor solubility and certain difficulties in their processing ⁵, limits their application in the field of paints and coatings. To overcome all such issues, several steps have been taken such as formulation of their composite materials through the addition of

CP fillers, dispersion and their copolymerization using chemical and electrochemical techniques, which synergistically enhances their performance. Among PANI derivatives, poly (o-anisidine) is one of the most significant members owing to its ease of synthesis, availability and cost effectiveness⁵. The o-phenyldiammine is considered as one of the prominent derivative of PANI⁶. The aromatic diammine based polymers are found to be more significant since they possess novel functionality of conjugation and terminal free amino groups in the repeating unit of their polymer chains. Furthermore, the copolymerization of o-phenyldiammine has remarkably improved some of the properties like stability, conductivity and solubility⁷. Literature revealed that many reports^{3, 8, 9} are available, on PANI, PPY, PTh, their derivatives and copolymers, which have exhibited promising anti-corrosive coating materials, e.g., Jadhav et al. synthesized PoA via emulsion polymerization and reported its dispersion in alkyd to develop its coatings on mild steel, which exhibited corrosion protection ability (I_{corr} for PoA/alkyd:0.48 $\mu\text{A}/\text{cm}^2$ and PANI/alkyd:0.4 $\mu\text{A}/\text{cm}^2$. in 5% HCl¹⁰. Chaudhari et al. have electrochemically synthesized polyethoxyaniline and studied its protective behaviour on carbon steel in 3% NaCl solution using EIS and potentiodynamic studies¹¹. Yao et al. have synthesized aniline-p-phenyldiammine copolymer and reported its corrosion protection performance using electrochemical measurements¹², their I_{corr} values in 5 % NaCl medium was found to be 0.06 $\mu\text{A}/\text{cm}^2$. Similarly, Ping et al. have demonstrated the synthesis and the formulation of aniline-p-phenyldiammine copolymer having TX-8 emulsifier using surfactant. They found that the composite coatings based on epoxy matrix possessed good corrosion resistance property¹³. Peng et al prepared PANI by conventional oxidative polymerization having leaf like morphology used as coating material and found that coatings exhibited high E_{corr} and low I_{corr} values¹⁴. All these works have encouraged us to develop a copolymer of o-anisidine and oPDA which possesses excellent

anti-corrosive properties analogous to those of the homopolymers, which has not been reported in the literature till, date. Thus, the aim of present work is to investigate the synthesis and characterization, physico-mechanical and anti-corrosive properties of PoA ad P(oA-co-o-PDA) copolymer nanocomposite coatings using epoxy-PA as a matrix. These studies revealed that the P (oA-co-oPDA)-epoxy-PA nanocomposite coatings have exhibited excellent anti-corrosion performance as compared to those of epoxy-PA, PoA-epoxy-PA and other such reported coating systems^{10, 12, 15-17}.

2. EXPERIMENTAL

2.1 Materials

Ortho-anisidine monomer (C_6H_9NO , M.W 123.16 g/mol and density 1.0923g/cm^3) Merck, Germany, o-phenyldiamine (1,2 Benzenediamine, $C_6H_8N_2$, M.W-108.14, M.pt. $101-103^\circ\text{C}$) ethyl methyl ketone, hydrochloric acid (HCl), S.D fine chem., Mumbai, Epoxy (DGEBA, D.E.R 332, epoxy equivalent 180–185, sp.gr. 1.2306, refractive index 1.5685, viscosity about 10,000 CP) DOW Chemicals, Ammonium peroxydisulphate (APS), Tergitol (NP-9) Sigma-Aldrich, USA, polyamide (PA) as curing agent (Aradur HY 840-1 EN, CAS No. 112-24-3, amine number 500-580) Shakar dyes, New Delhi, India and were used as received. All chemicals were of analytical grade and used as recieved.

2.2 Synthesis of PoA nanoparticles and P(oA-co-oPDA) copolymer nanorods

2.0 g of o-anisidine was taken in a three necked flat bottom flask containing 100 ml of 0.1 M HCl along with magnetic bar and kept on a magnetic stirrer. The 30 ml solution of APS in 1M HCl was dropwise added to the above reaction mixture, simultaneously, the 30 ml solution of 0.5 g Tergitol-X (NP-9) in 1M HCl was added to the reaction mixture, followed by the reaction under continous stirring at ambient temperature (30°C) for 6 h and allowed to further proceed for 24 h at

sub-zero temperature (0-5 °C) in an ice bath. The progress of the reaction was monitored by the change in colour of the solution of the reaction mixture i.e from dark green to black and FT-IR spectra, which was taken at regular intervals of time. At the end of the reaction, the black coloured PoA nanoparticles were formed, which was filtered and washed several times with methanol to remove the unreacted moieties, dried in vacuum oven at 70 °C for 2 days at 10 mm pressure.

The synthesis of black coloured P(oA-co-oPDA) copolymer nanoparticles was performed using the same reaction set-up and procedure used for PoA. The 1.10 g of o-phenyldiammine monomer was added in the reaction mixture used for PoA, and the reaction was carried out accordingly. On the completion of the reaction, the black colour nanorods (100-120nm) were formed as per the scheme 1. The formation of PoA nanoparticles and P(oA-co-oPDA) nanorods were confirmed by TEM studies. The yield % of the vacuum dried PoA and P(oA-co-oPDA) were found to be 68 % and 71% respectively.

2.3 Preparation of PoA-epoxy-PA and P(oA-co-o-PDA)-epoxy-PA nanocomposites

The PoA-epoxy and P(oA-co-o-PDA)-epoxy nanocomposites were prepared using different loading of PoA (1.0, 1.5 and 2 wt. %) and P(oA-co-o-pda)(1.0, 2.0 and 3.0 wt. %) by solution blending technique in the solution of 80 wt. % of epoxy in ethyl methyl ketone. The dispersion of these nanofillers in epoxy matrix was performed by ultrasonication for 30 min and 20 min followed by the mechanical stirring for 8 h and 5 h respectively at room temperature, resulted in the formation of a homogeneous composite solution. The nanocomposite solutions were kept under observation for a fortnight to see if there was any phase separation or not. However, no such separation was observed. The loading of P(oA-co-oPDA) in epoxy showed uniform

dispersion only upto 3.0 wt. % while that of PoA is upto 1.5 wt. %. Beyond these loadings, agglomeration and phase separation was observed in both the cases.

2.4 Formulation of nanocomposite coatings

The 30phr PA was homogeneously mixed in the 80 wt. % solutions of epoxy, PoA-EMK and P(oA-co-o-PDA)-epoxy in EMK (Fig. 1b) . Their coatings were prepared by brush technique on finely polished washed and rinsed CS strips of standard sizes. These coatings were cured at room temperature with in 12 h, 5 h and 45 min respectively. The average thickness of coatings was found around 130 μm . The minimum curing time in case of P(oA-co-o-PDA)-epoxy-PA nanocomposite coatings can be attributed to the presence of $-\text{NH}$ groups that enhances the condensation curing reaction.

2.5 Characterization

The structural elucidation of PoA nanoparticle, P(oA-co-o-PDA) copolymer nanorods, epoxy-PA and their nanocomposite was carried out using Fourier transform infrared (FT-IR) taken on a PerkinElmer 1750 FT-IR spectrophotometer (PerkinElmer Instruments, Norwalk, CT) in the form of KBr pellets, and ^1H - NMR on JEOL GSX 300 MHz FX-100 in DMSO using TMS as the internal standard. UV-Visible spectra were taken on Perkin-Elmer-Lamda-Ez-221. The particle size and surface morphology analysis were carried out by Transmission electron microscopy (TEM) model Morgagni 268-D TEM, FEI, USA operated at an accelerated voltage of 120 kV. Scanning Electron Microscopy (SEM) was carried out on model FEI Quanta 200F with Oxford-EDS system IE 250 X Max 80. BET analysis was conducted with the help of Quanta Chrome instrument (model NOVA 2000e USA) using nitrogen gas environment to determine the surface area of P(oA-co-oPda). The crystalline nature and phase purity were investigated using X-ray

diffractometer model Philips W3710 and $\text{CuK}\alpha$ radiation. Thermo gravimetric analysis (TGA) was performed on the SII EXSTAR 6000 thermal analyzer (Japan) from 40 °C to 800 °C under nitrogen environment at a flow rate of 10 ° C/min. Hydrophobic behaviour of coatings was evaluated by contact angle measurement using drop Shape Analysis System (model DSA10MK2Kruss GmbH, Germany) with high speed CCD camera for image capture¹⁸. The carbon steel specimen were polished successively with different grade of emery papers (600–800–1000) and were washed thoroughly with double distilled water, degreased with methanol and acetone and dried at room temperature. These coating materials were applied by brush on the finely polished CS strips (2.87% C and 97.13% Fe) of standard size (70×30×1 mm³) used for the determination of physico-mechanical properties of specular gloss at 45 ° by a gloss meter (model RSPT-20, digital instrument Santa Barbara, CA), scratch hardness test (BS 3900), bend test on 1/8" inch conical mandrel (ASTM D 3281-04), cross-hatch test (ASTM D3359), methyl ethyl ketone (MEK) solvent rub resistance test (ASTM D5402) and impact resistance test (IS: 101 par 5/sec-31988). The conductivity was measured by the standard four probe method using a Keithley DMM 2001 and EG and G Princeton Applied Research potentiostat model 362 as a current source. For each value, three specimen were used for the measurement of conductivity. The mean averages of five values of the conductivity were taken. Corrosion resistance performance of the P(oA-co-o-PDA)-epoxy-PA, PoA-epoxy-PA and epoxy-PA coated CS strips were evaluated by potentiodynamic polarization measurements and electrochemical impedance spectroscopy in NaCl (5 wt %) and HCl(5 wt %) at room temperature (30°C) using micro Autolab type III with FRA unit (μ 3AVT 70762, Netherlands) potentiostat. The Tafel plots in presence of above said corrosive media were obtained using a three-electrode electrochemical cell (EG&G 362) containing platinum gauze as counter electrode, Ag/AgCl as reference

electrode and test specimen (coated and uncoated carbon steel specimen) as working electrodes. The test specimen were fitted in electrochemical cell with 1cm^2 area of the sample exposed to the corrosive media¹⁹. The potentiodynamic polarization tests were carried out in the potential range ± 100 mV (with respect to OCP) at 0.001 mV/s scan rate. Nova 1.8 software was used for data fitting and calculation of results. The impedance and Tafel parameters were determined by curve fitting programme available in the said software. Each test was run in triplicate to verify the reproducibility of the data.

3. Results and discussion

Structural elucidation

3.1 FT-IR Analysis

The FT-IR spectrum (Fig. 2a-b) of P(oA-co-oPDA) showed the presence of an intense NH stretching vibration (ν_{str}) band at $3,350\text{ cm}^{-1}$. The C=N (ν_{str}) and C=C (ν_{str}) stretching bands for the quinonoid (Q) and benzenoid (B) rings appeared at $1,595\text{ cm}^{-1}$ and $1,505\text{ cm}^{-1}$ respectively. The peak at $1,244\text{ cm}^{-1}$ was assigned to the C–N stretching peak for the benzenoid rings, and peak at 1256 cm^{-1} showed C–O aromatic peak of benzene ring. The C–H bending vibration formed during protonation was confirmed by the presence of peak at 1112 cm^{-1} . The C–O–C peak for ether group at 1147 cm^{-1} was observed. The other band at 848 cm^{-1} revealed the presence of phenazine units²⁰. The band at 754 cm^{-1} revealed the presence of 1, 2 substitutions of NH_2 group at 1st position and OCH_3 group at 2nd position respectively. The absorption bands of PoA had all peaks except the phenazine unit as depicted in earlier study¹⁰. The bands at 820 cm^{-1} is used as an inner criterion, the band of N–H stretching mode (3350 cm^{-1}) in P(oA-co-oPDA) copolymer was found stronger than PoA. This implies that P(oA-co-oPDA) contains more end capped

amino groups. In addition, bands at about 742 cm^{-1} and 692 cm^{-1} were observed in P(oA-co-oPDA) which confirmed the presence of P(oA-co-oPDA) oligomers. The absorption bands of PoA had all characteristic peaks except the phenazine unit, which suggests the formation and confirmation of copolymer.

The FT-IR spectrum (Fig. 2), of epoxy showed a characteristic band at $3,449\text{ cm}^{-1}$ associated with broad OH stretching of the hydroxyl groups. The peaks appearing in the range of $1,296\text{--}1,184\text{ cm}^{-1}$ were correlated to the C–O–C of aryl alkyl ether, while the peak at $1,095\text{ cm}^{-1}$ was attributed to the aryl alkyl ether symmetric stretching (sym). The oxirane ring peaks appeared at $910\text{--}830\text{ cm}^{-1}$.

The FT-IR spectrum (Fig. 2), of 2.0% P (oA-co-oPDA)-epoxy showed OH stretching vibration peak at $3,460\text{ cm}^{-1}$ broader in wavelength, which shifted by 14 cm^{-1} as compared to epoxy matrix. The presence of peaks at $1,390$, $1,438$ and $1,508\text{ cm}^{-1}$ corresponded to the benzenoid and quinonoid stretching modes of P(oA-co-oPDA). The benzenoid and quinoid vibration peaks were very intense and pronounced indicating the strong interaction between P(oA-co-oPDA) and epoxy. These bands suggested a conjugation pi-bond system, which may be attributed to the doped state of P(oA-co-o-pda)⁸. As the doping improves conductivity levels forming polaron/bipolaron structures resulting in the increase of charge transfer in P(oA-co-opda) and also the higher electronic delocalization. The presence of conjugated double bonds in the benzenoid and quinonoid rings permits electron mobility throughout the P(oA-co-opda) chains, responsible for more electron delocalization, which resulted in the conducting nature of nanocomposite. The NH stretching vibration band of P (oA-co-oPDA) overlaps the OH stretching vibration which revealed the electrostatic interaction of NH group of P (oA-co-oPDA) and OH group of epoxy via strong hydrogen bonding^{21, 22}. All other peaks, which corresponded to epoxy, did not exhibit

any major shift. Hence, the formation of P(oA-co-o-PDA)-epoxy as nanocomposite was confirmed.

3.2 NMR analysis

The ^1H NMR (Fig.3, ESI: Fig.1a-b) of P (oA-co-oPDA) revealed the presence of peaks between $\delta=6.6$ and 7.4 ppm, which corresponded to the aromatic protons. Similarly, the ^1H NMR spectra of PoA reported in earlier study²³ have characteristic peak in this region but of slightly less intensity. The peak at $\delta=3.4$ ppm correspond to OCH_3 group and the two peaks at $\delta= 3.7$ ppm for $-\text{NH}$ and $-\text{NH}_2$ ¹². The singlet signal at $\delta=2.5$ ppm were correlated to the solvent protons.

3.3 UV-Visible analysis

The UV-visible spectra (Fig.4) of P (oA-co-oPDA) revealed the presence of characteristic peaks at 260 nm and 285 nm, which was assigned to $\pi-\pi^*$ transition in benzenoid ring. The peak at 430 nm was assigned for donor acceptor interaction of quinoid amine units ($-\text{C}=\text{N}-$)²⁴.

Particle size, morphology and surface area

3.4 TEM and SEM/EDAX analysis

The formation of tubular shaped P(oA-co-oPDA) nanorods of dia. ca. $100-120$ nm was confirmed by TEM analysis (Fig.5a) approaching to nano scale²⁴. The SEM studies (Fig.5b-d) ESI:Fig.2 were in concordance with TEM results showing the presence of nanorods of specific morphology, EDAX (Fig.5 d) analysis clearly confirmed the presence of N, C, H elements etc in nanorods. The TEM micrograph (Fig. 5e) of PoA a homopolymer showed well dispersed rice shaped nanoparticles of dia $25-30$ nm. The TEM micrograph of P(oA-co-o-PDA)-epoxy-PA nanocomposite (Fig. 5f) showed well dispersed P(oA-co-oPDA) nanorods of ($90-95\text{nm}$) size within the epoxy-PA matrix. The electrostatic interaction of NH groups of nanofiller and that of

PA with oxirane groups of epoxy lead to the formation of physical bond between filler and matrix, which confirmed, the formation of nanocomposites. The improved properties of P(oA-co-o-PDA)-epoxy-PA nanocomposite can be correlated to the presence of doped nanorods, which were homogeneously dispersed within the polymer matrix and effectively induced adhesion between the nanocomposite coating and metal surface through the electrostatic interaction of positively charged metal surface with those of negatively charged pendant groups of matrix resulting into the formation of well-adhered homogeneous and compact coating on CS surface.

3.5 BET analysis

BET analysis of P (oA-co-oPDA) nanorods confirmed the porous nature and higher surface area of nanorods. The average surface area was found to be 281.30 m²/g and pore size 1.51 Å .The porous nature of nanorods has suggested that these particles may also have potential for their applications in the field of adsorption and catalysis reactions. The nano scale porosity had introduced nanoscale roughness in the coating materials, which resulted in the enhanced the hydrophobicity and reduced wettability of coating surface that improved the corrosion protective efficiency of coatings ²⁵.

Crystalline nature

3.6 X-Ray Diffraction

X-ray diffraction studies was performed to analyse the crystalline structure and phase identification of P(oA-co-opda).XRD diffractogram (Fig. 6) showed pronounced peak at $\theta = 22^\circ$ and 25° , which can be correlated to (0 2 0) reflection ²⁶ and local crystallinity. A broad band centred at $2\theta = 11^\circ$ and 15° , which revealed the partial crystalline nature of the nanorods that might caused by NH₂ (amine) groups present perpendicularly within the polymer chain

resulting in the formation of semi-crystalline, short range nanorods particularly in case of HCl doped CPs. Thus confirming the semi-crystalline nature of copolymer as concordance with X-Ray results while XRD diffractogram of PoA as given in earlier study²⁷ showed a broad hump, spanning between $\theta = 20^\circ$ and 30° responsible for its amorphous nature.

3.7 Solubility Test

The solubility of epoxy (matrix), PoA nanoparticles, P(oA-co-oPDA) copolymer and their nanocomposites were investigated in various polar and non-polar solvents at room temperature. The P(oA-co-opda) copolymer was well dispersed in polar solvents such as methyl alcohol, ethyl alcohol, DMSO, DMF and NMP than that of non-polar solvents. This can be attributed to the presence of –NH groups and oxygen atoms in P(oA-co-opda), which is more electronegative and has lone pair of electrons that induces electrostatic interaction between oxygen and hydrogen atoms of the constituent moieties²⁸. Thus, hydrogen atoms of organic solvents were attracted to the lone pair electrons of negatively charged oxygen atom present in P(oA-co-oPDA) to form the hydrogen bond. This can be correlated to the lone pair orbital of oxygen atom projected within the space away from the positively charged nuclei, promoting a considerable charge separation. Hence, the higher dispersion was observed in polar solvents as compared to non-polar solvents. The solubility of PoA nanoparticles in polar solvents was found lower than that of P(oA-co-opda) copolymer. Similarly in case of epoxy matrix and P(oA-co-o-PDA)-epoxy-PA nanocomposites, which have polar hydroxyls, oxirane, and amino moieties exhibits enhanced solubility in polar solvents like methanol, ethyl methyl ketone, DMSO, NMP but partially soluble in acetone (Table 1).

Thermal stability

3.8 Thermal analysis

TGA and DSC analysis were performed to examine the thermal stability of polymer. TGA with DTG and DSC curves are shown in Fig.7. The P (oA-co-PDA) copolymer showed three step decomposition process.

The initial loss of (5-10 %) upto 120°C can be attributed to the evaporation of superficial moisture, other volatile compounds, intermediate oligomers, as well as unreacted monomer elimination. Then, at higher temperatures from 180°C-280°C, the second weight loss (55-70%) occurred, which can be attributed to the aliphatic and protonic acid component of the polymer²⁹ which was lost at this temperature range. This was also attributed to the removal of dopants (Cl-), low oligomers or side products as well as to the destruction of NH+....Cl- interaction between PoA chain and Cl- dopant in this temperature range³⁰. The third sluggish decomposition (wt. loss 60 %) in the said region (range 420-800°C) was assigned to the degradation of backbone units of oPDA benzenoid and quinoid units²⁴ along with -NH₂ moiety with benzene ring chain and finally at more extreme temperature the polymer chain breaks lead to production of various gases such as C₂H₂ or NH₃. All results were in concordance with DSC data (Fig 7) which possess three exotherm at these temperatures responsible for three stage decomposition of P (oA-oPDA) nanorods (AFM image ESI: Fig 3) .

DSC gives information on the energy absorbed or liberated during the thermal treatment of the polymers. This study indicated that three exothermic reactions occur between 250 °C and 400 °C. The exothermic reaction suggests that the formation of higher cross-linked P(oA-co-oPDA) copolymer formed . The energy released at around 280 °C in second step can be corroborated to breaking of NH+....Cl- interaction between PoA chain with Cl dopant .

The third exotherm at around 420 °C, can be ascribed to the degradation of backbone units of oPDA benzenoid and quinoid units along with –NH₂ moiety respectively³¹.

3.9 Conductivity studies

The conductivity of CP mainly depends on the number of charge carriers and the conjugation length within the polymer backbone. The conductivity measurements were carried out under ambient conditions. The conductivity of pristine PoA was found to be 5.02×10^{-3} S/cm while that of oPDA was found to be 1.1×10^{-7} S/cm. On the other hand, the conductivity of P(oA-co-oPDA) copolymer was found to be 4.2×10^{-2} S/cm, which was more comparable with that of PANI. The conductivity of o-pda was low due to the bulky-NH₂ substituent's/groups that are present in the polymer, which roots the main chain twisting. The literature revealed, that the conductivity of the copolymer containing PoA and oPDA decreases with the increased loading of o-PDA polymer in the co-polymer P(oA-co-oPDA) which was present in low content (0-20 mol % only). As literature depicts, that the conductivity of the copolymer containing PoA and oPDA decreases with the increase in content of o-PDA polymer in it. This further reduced its co planarity and resulted in a barrier to interchain allocation and jumping of e⁻s thereby shortening the conjugation length.

3.10 Surface wettability test

The hydrophobic behavior of coatings was analysed by deionized water for the evaluation of hydrophobic properties of the coated substrate. Angle measurements were done in triplicates. Water was taken in the syringe and its drops (15 µl) were allowed to fall on the substrate, the left and right contact angles were measured for 10s at 1s interval. The average contact angle was calculated by using the three values of left and right contact angles. The CCD camera images of

water droplets on the surface of coatings are shown in Fig 8. The contact angle analysis revealed that the highest value was observed in copolymer (PoA-co-oPDA)-epoxy-PA nanocomposite coatings (92°) followed by (PoA-epoxy-PA) (79°) and epoxy-PA coatings (62°). The highest contact angle value for co-polymer nanocomposite coatings can be attributed to the presence of higher roughness at nanoscale that lead to the formation of air pocket within the coating which were responsible for the decrease in wettability³². Hence the amplified contact angle accountable for the improved hydrophobicity of coatings, which is considered to be an important parameter required for effective anticorrosive behaviour of coatings³³.

3.11 Physico-mechanical properties

The physico-mechanical properties of epoxy-PA, PoA-epoxy-PA and P(oA-co-oPDA)-epoxy-PA coated CS are given in Table 2. The average coating thickness was found to be epoxy-PA (110-120 μm), PoA-epoxy-PA (120-125 μm) and P(oA-co-oPDA)-epoxy-PA (125-135 μm) nanocomposite coatings respectively. The scratch hardness values found to increase in the order P(oA-co-oPDA)-epoxy-PA (12.9 kg) > PoA-epoxy-PA (9.7 kg) > epoxy-PA (6.5 kg) coatings, this trend can be correlated to the extent of cross-linking which restricted the indentation. The improved scratch hardness values of the coatings can be attributed to the ladder structure of P(oPDA) polymer³⁴. The high scratch hardness value of P(oA-co-oPDA)-epoxy-PA coated samples can also be correlated to the enhancement in the adhesion between P(oA-co-oPDA)-epoxy-PA coatings and metal substrate. The enhanced adhesion between the epoxy-PA, PoA-epoxy-PA and P(oA-co-oPDA)-epoxy-PA coating with CS respectively was further confirmed by the cross-hatch test. The optical images (Fig. 9(a-b)) of coated CS before and after cross hatch test showed no spalling of coating was observed in case of P(oA-co-oPDA)-epoxy-PA while spalling was observed in case of PoA-epoxy-PA and epoxy-PA coatings. No change in

gloss of these coatings was found that can be attributed to their opaque nature and black colour. Both PoA-epoxy-PA and P(oA-co-oPDA)-epoxy-PA coatings passed the impact test. This revealed that the coatings absorbed the highest limit of impact energy due to the presence of long chain carbon flexible moieties like polar hydroxyls and oxirane functionalities present in the backbone of the polymeric chain of nanocomposites along with the presence of strong hydrogen bonding³⁵. The flexibility of the coatings was determined by the bending test with the help of conical mandrel. The coatings were found to be flexible as they bend without any damage or fracture. The MEK double rub cycle test values of all the coated CS are given in Table 2 were higher than 400 cycles. The physico-mechanical performance of 3.0 wt. % of P(oA-co-oPDA)-epoxy-PA and 1.5wt. % of PoA-epoxy-PA coatings were best among all the ratios prepared of these coatings and were further analysed for their corrosion protective performance using advance techniques like PDP and EIS electrochemical studies.

Corrosion studies

3.12 PDP studies

The potentiodynamic polarization experiments were conducted for quantitatively analysis of the anticorrosive performance of P(oA-co-oPDA)-epoxy-PA, PoA-epoxy-PA, epoxy-PA coated CS and bare CS (Fig. 10a-b). The electrochemical parameters such as corrosion current density (I_{corr}), corrosion potential (E_{corr}), β_{anodic} and $\beta_{cathodic}$ (Tafel slopes b_a and b_c) of the coated and uncoated CS was investigated with the help of potentiodynamic polarization curves as given in Fig.10 and Table 3. The below given Stern-Geary equation³⁶ was further used to calculate the polarization resistance R_p and b_a and b_c values ($dE/d\log I$)³⁷

$$R_p = \frac{babc}{2.303 (b_a + b_c) I_{corr}}$$

Fig.10 (b) shows the polarization curve of epoxy-PA, PoA-epoxy-PA and P(oA-co-oPDA)-epoxy-PA, coated CS in 5 wt. % NaCl. The CS samples coated with pure epoxy-PA exhibited the lowest corrosion potential and the highest corrosion current density while, the PoA-epoxy-PA coatings had higher corrosion potential and lower corrosion current density values in comparison, to that of epoxy-PA coatings. On the other hand, P(oA-co-oPDA)-epoxy-PA nanocomposite coatings have exhibited significantly higher corrosion potential E_{corr} and lowest I_{corr} among all these coatings. The trend of E_{corr} was found to be CS < epoxy-PA < PoA-epoxy-PA < P(oA-co-oPDA)-epoxy-PA, which confirmed that the P(oA-co-oPDA)-epoxy-PA, copolymer composite coatings had considerably higher corrosion protection to CS in saline environment. The superior corrosion protection of P (oA-co-o-pda-epoxy-PA), coatings to CS may be correlated to the fact that the nanofiller were homogeneously dispersed in matrix. The polar pendant functional groups of nanorod filler and that of epoxy induced adhesion at coating-CS interface ²¹. These polar groups developed strong electrostatic interaction between labile positive charge present on the metal surface, and negative charged pendant groups of coating resulted in strong adhesion at coating metal interface. The other reason may also be the presence of the hydrogen bonding between the matrix and filler which lead to the reduction in the effective area of corrosion through the blockening of reaction sites.

Similarly, the PDP studies in 5 wt. % HCl solution (Fig. 10a), revealed the performance of bare CS, epoxy-PA, PoA-epoxy-PA, and P(oA-co-oPDA)-epoxy-PA coating followed the same trend as discussed above in case of 5 wt. % NaCl solution (Fig. 10a(A-D)). The highest corrosion resistance behaviour of P(oA-co-oPDA)-epoxy-PA coatings in HCl can be attributed to these two reasons, first the blocking effect of Popda, a ladder polymer possessing phenazine skeleton

molecular structure³, which blocked the transport of moisture, oxygen and other corrosive moieties to the coating metal interface, resulted in the effective reduction in corrosion kinetics. Further, the nanofiller also induces healing and locking effect³⁸ in coatings that enhanced the corrosion protective performance of P(oA-co-oPDA)-epoxy-PA composite coatings in HCl medium which was further confirmed by the lower I_{corr} and higher E_{corr} and R_p values of P(oA-co-oPDA)-epoxy-PA coated CS as compared to PoA-epoxy-PA, epoxy-PA and bare CS. This can be correlated to the formation of passive compact iron/dopant complex layer at the metal-coating interface, which has the capability for the continuous charge transfer reaction at the metal-coating interface that provide protection to CS under saline and acidic environment³⁹. Mobin et al have chemically developed Poly (aniline-co-o-toluidine) and Poly (pyrrole-co-o-toluidine) based conducting polymers coatings on MS and has studied their anti-corrosive protection performance under low concentration of corrosive ions i.e. 0.1 M HCl while the present study reports in 5 % HCl (1.3 M HCl) solution. Hence, on comparison, we found that the performance of our system was far superior to those developed by Mobin et al.^{15, 16}

3.13 EIS studies

Dielectric spectroscopy (often called impedance spectroscopy and also known as electrochemical impedance spectroscopy), measures the dielectric properties of a medium as a function of frequency. It is also an experimental method of characterizing electrochemical systems. This technique measures the impedance of a system over a range of frequencies, and therefore the frequency response of the system, including the energy storage and dissipation properties, is revealed. Often, data obtained by EIS is expressed graphically in a Bode plot or a Nyquist plot. In this study, the corrosion potential E_{corr} , I_{corr} and impedance were measured. The impedance spectroscopy is a non-destructive technique used to determine the several electrochemical parameters measured in this study like degree of coating degradation, coating capacitance and resistance, which are related to the extent of water and ion

absorption ability respectively. The relative anti-corrosive performance of nanocomposite coatings was investigated using the electrochemical impedance spectroscopy (EIS) study which was conducted in 5 wt. % NaCl and 5 wt. % HCl media. The measurements were performed after coatings were dipped for a period of 6 h to attain proper stabilization of the system. Fig. 11a gives the best fit equivalent circuit in NaCl and HCl corrosive environments, which comprised R_s (solution resistance), R_{pore} (pore resistance) and C_c (coating capacitance). The high frequency intercept was found equal to the solution resistance, and the low-frequency intercept to be equal to the sum of R_s and R_{pore} as shown in Fig. 11b(A-D), Fig. 11c(A-D) and Table 3b depicts the Nyquist plots and their values for CS samples coated with pure epoxy-PA, PoA-epoxy-PA and P(oA-co-oPDA)-epoxy-PA nanocomposite coatings in 5 wt.% NaCl and 5 wt.% HCl media, respectively. All Nyquist plots were close to a semicircle, which contained one time constant and the diameter of which was equal to the charge transfer resistance (R_{ct}) for P(oA-co-oPDA)-epoxy-PA coatings while the formation of higher semicircle diameter, confirmed the low corrosion rate of coatings.

In case of, 5 wt. % NaCl solution (Fig. 11 c),, it was found that the value of R_{ct} gradually increased to higher value with the increase in the content of nanofillers in coatings, R_{ct} of P(oA-co-oPDA)-epoxy-PA approached to the highest value as compared to PoA-epoxy-PA and epoxy-PA coatings. Literature has also revealed that once the CPs like PANI⁵, PPy⁴⁰, and their derivatives⁴¹ are introduced, coating resistance could be maintained at relatively higher values, indicating the better protection performance of CP containing coatings than that of pure epoxy coatings³⁵. This clearly indicated that the introduction of PoA and P(oA-co-oPDA) in epoxy matrix further enhanced the anti-corrosive performance of epoxy-PA coatings. The EIS studies of these coatings showed that the highest R_{pore} values⁴² and lower C_c values for P(oA-co-

oPDA)-epoxy-PA nanocomposite coatings was observed than those of PoA-epoxy-PA and epoxy-PA coatings. During the entire immersion period, the increasing trend of R_{pore} varies as CS (1.2×10^3), epoxy-PA (2.2×10^4), PoA-epoxy-PA (1.27×10^6) and P(oA-co-opda)-epoxy-PA (1.72×10^7) respectively, which clearly confirmed the best anti-corrosive performance of copolymer coatings⁴². The reason for higher corrosion protection efficiency of P(oA-co-oPDA)-epoxy-PA nano composite coatings were well explained in the preceding section (PDP studies). It was also found that the value of C_c gradually became lower with incorporation of the P (oA-co-opda), nano-fillers in epoxy matrix as the trend observed was epoxy-PA (2.32×10^{-4}), PoA-epoxy-PA (9.67×10^{-6}), and P(oA-co-oPDA)-epoxy-PA (7.9×10^{-10}) coatings respectively⁴³.

In case of 5wt. % HCl medium (Fig. 11 b), that is the higher increase in R_{pore} and decrease in C_c values of P(oA-co-oPDA)-epoxy-PA coatings as compared to PoA-epoxy-PA and epoxy-PA coatings. The similar performance was observed here as in case of 5wt. % NaCl coatings. The trend after immersion was observed as the increasing trend observed was epoxy-PA (6.1×10^3), PoA-epoxy-PA (2.3×10^5), and P(oA-co-oPDA)-epoxy-PA (3.1×10^7) coatings respectively. It has been observed that when coatings dipped in HCl solutions, they doped with anion Cl^- and the exchange of doped Cl^- ions of doped and undoped mechanism of CP maintains overall neutral environment to nanocomposite coatings. In HCl medium, when the CS coated with copolymer coating was immersed, the anions doped in the copolymer (Cl^-) can be exchanged with the Cl^- ions of the medium. After that, the process was accompanied with the oxidation and reduction of the copolymer and small ions were doped into and dedoped out of the copolymer, respectively to maintain the overall neutral behaviour. Under this situation, plenty of dopant ions and the anions of the solution were excluded from the copolymer and the CS substrate was protected against the localised corrosion by chloride ion attack² Table 3(b).

Bode plots of epoxy-PA, PoA-epoxy-PA and P(oA-co-oPDA)-epoxy-PA, coated CS in 5 wt % NaCl and HCl are given in Fig. 11d-e, respectively. The Bode plot (Fig. 11d (A-D) in NaCl medium shows that the impedance value of the coated CS increased from 10^3 to 10^8 ohm with the addition of conducting filler PoA and further increase this value with its copolymerization with o-PDA. The same behaviour of the Bode curves was also observed in 5wt. % HCl media (Fig.11e). Murray et al ⁴⁴ proposed that the Z_{max} value of the low-frequency region in the Bode diagram played an important role in characterizing the anti-corrosion performance of coatings. The Z_{max} value was found to higher, due to the stiff and dense nature of composite coatings, which implies better barrier to CS from corrosion ions. The increase in R_{pore} and decrease in C_c value ⁴³ clearly depicted that the incorporation of conducting copolymer fairly increased the anti-corrosion performance of composite coatings. The impedance behaviour in CP can be best explained by the intermediate redox reaction i.e. the dispersed P(oA-co-oPDA) particles in nanocomposite coatings provided passivation to the metal surface through the interaction between P(oA-co-o-pda)and epoxy with the underlined CS, also P(oA-co-o-pda) re-oxidise itself by dissolved oxygen ^{42, 43}.

Fig. 11e(A-D) shows the Bode plots of CS samples coated by P(oA-co-oPDA)-epoxy-PA, with various amounts of P(oA-co-oPDA)-epoxy-PA, in 5 wt% HCl. It was found that the Z_{max} in low-frequency region gradually increased from epoxy-PA to PoA-epoxy-PA and finally to P(oA-co-oPDA)-epoxy-PA, copolymer coatings. This indicated that the introduction of P(oA-co-oPDA) in epoxy provided promising corrosion protection to CS. The values of R_{pore} significantly increased as epoxy-PA (6.1×10^3), PoA-epoxy-PA(2.3×10^5), and P(oA-co-oPDA)-epoxy-PA (3.1×10^7) coatings respectively. Thus, composite coating containing P(oA-co-o-PDA)-

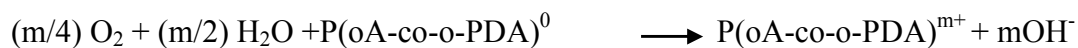
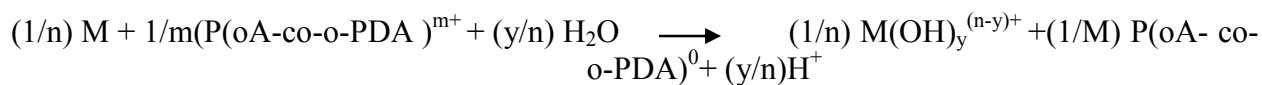
epoxy-PA exhibited the lowest ion diffusion and the best barrier property to CS exposed to severe acidic and saline corrosive environments ⁴⁵.

3.14 Salt spray test

The salt spray test of P(oA-co-o-PDA)-epoxy-PA, PoA-epoxy-PA, neat epoxy-PA coated and uncoated CS was conducted for a period of 360 h in 5 wt. % NaCl. The uncoated CS was treated as control, in neat epoxy-PA coating deterioration started after 120 hour, while in case of PoA-epoxy-PA coated CS, the sign of slight deterioration was observed, and no accountable observation in case of P(oA-co-o-PDA)-epoxy-PA coated CS. The micrograph revealed the presence of uniform, thick and compact morphology of P(oA-co-o-PDA)-epoxy-PA coating, which can be correlated to the higher corrosion resistance performance of coated CS. This can be attributed to the promising corrosion resistance performance of P(oA-co-o-pda)-epoxy-PA, coating in NaCl medium. As, the conducting polymer content was increased in epoxy, hydrophobic surface with increased crosslink density formed, which did not allow corrosive ions to wet the surface, thus increasing the corrosion resistance performance of the P(oA-co-o-pda)-epoxy-PA, coating as compared to bare CS. Further, these explanations were also well supported by PDP and EIS studies.

3.15 Mechanism of corrosion protection

The corrosion protection mechanism of conducting polymers present in insulating coatings is mainly dependent on three factors, firstly the formation of passive layer, barrier effect and adhesion¹⁴. The mechanism of the corrosion protection of CS provided by CPs is well reported in the literature ⁴⁶. It was considered that the conducting moieties of these polymers acted as an active coating in the reaction taking place across the polymer coated and metal-electrolyte interface as explained by Kinlen et al ⁴⁶ using the below given equation,



The formation of iron oxide layer at the coating metal interface improved the corrosion protection by the dispersion of copolymer in coatings. The presence of the passive layer was confirmed by Raman spectra. As shown in Fig. 13, the bands on the surface of P(oA-co-oPDA)-epoxy-PA copolymer and epoxy-PA coated CS immersed for 15 days in 5 wt % NaCl aqueous solution were investigated. The presence of 526 cm^{-1} was assigned to chlorination of P(oA-co-o-PDA)-epoxy-PA, the absence of such modification in epoxy without conducting polymer filler may be an indication of the structural changes observed in epoxy as induced by filler and they improved the corrosion protection performance as also reported in literature. The detail assignment of peaks is shown in Table 4. The bands at about 216, 281, and 1293 cm^{-1} were assigned to $\alpha\text{-Fe}_2\text{O}_3$ [Fig.13]. This indicates that the surfaces of CS coated by P(oA-co-oPDA)-epoxy-PA formed the passive layer of $\alpha\text{-Fe}_2\text{O}_3$. Further Raman spectroscopy also depicted some kind of interaction between epoxy matrix and P(oA-co-o-pda) copolymer filler. During the immersion in media an oxidation of Fe to Fe^{2+} and Fe^{3+} takes place through the formation of the passive oxide layer. In this case, the oxidation was accompanied by the reduction of PoA-co-o-PDA-ES (emeraldine salt) to PoA-co-o-PDA-LS (leuco-emeraldine salt) forming a passive layer following the mechanism of PANI. Because of this passive layer, copolymer coatings were able to offer high corrosion resistance, as evident from EIS. Here, in case of P(oA-co-o-PDA)-epoxy-PA coatings the presence of P(oA-co-oPDA) copolymer in the epoxy matrix provides two step mechanism acting as a barrier. Moreover, as PoA copolymerize with PoPDA which is a ladder polymer having molecular structure with phenazine skeleton along with assymetrical quinoid

structure which ensured greater adsorption of copolymer in epoxy-PA matrix on CS surface. It also decreased the effective area for the corrosion reaction by blocking the reaction sites and the presence of pi electrons in the aromatic ring co-existing with quaternary nitrogen atom²⁰. Anodically produced Fe³⁺ ions form metal coordinate ligand with hetero atoms (nitrogen and oxygen) present in PoPD. Subsequently, the cathodic reaction was suppressed due to the lack of electrons. Moreover, the conductivity of the copolymer layer affects the oxidative tendency, which brought about the passive state. On the above, the excellent adhesion of P(oA-co-o-PDA)-epoxy-PA nanocomposite coatings, with the metal substrate due to the uniform dispersion of P(oA-co-o-PDA) nanoparticles in a matrix as evident from SEM/EDX study (Fig.12b), which can be corroborated for the superior anti-corrosive performance. Based on these observations, the suitable mechanism has been presented in the graphical abstract.

4. Conclusion

P(oA-co-o-PDA) nanorods and PoA nanoparticles were synthesized via emulsion polymerization and their nanocomposites were prepared using epoxy-PA matrix by solution blending method. P(oA-co-o-PDA) copolymer nanorods were characterized by FTIR, ¹H-NMR, XRD, UV-visible, SEM and TEM. The nanocomposite coatings have exhibited enhanced physico-mechanical properties in comparison to virgin epoxy and bare CS, owing to uniform dispersion of nanostructures in epoxy matrix. The contact angle, salt spray test, potentiodynamic polarization revealed that the P(oA-co-o-PDA)-epoxy-PA acted as hydrophobic and protective coating on CS against corrosion in NaCl and HCl media (5 wt %). The Raman spectroscopy revealed the presence of passive ferric oxide layer, which induces remarkable effect in P(oA-co-o-PDA)-epoxy-PA composite coatings. The studies revealed that the nanocomposite coatings exhibited

outstanding anti-corrosive properties as compared to other such reported CPs based coatings. Further studies, such as effect of pH, are under progress.

ACKNOWLEDGEMENTS

Neha Kanwar Rawat is thankful to the University Grants Commission (UGC-BSR), New Delhi, India, for financial support in this work. Authors also acknowledge to SAIF centre, All India institute of Medical Science (AIIMS) and AIRF, Jawaharlal Nehru University, New Delhi. The authors are grateful for the TGA facility under the UGC, SAP of the Department of Chemistry, JMI, and New Delhi, India.

References:

1. T. Tüken, B. Yazıcı and M. Erbil, *Progress in Organic Coatings*, 2005, **53**, 38-45.
2. Y. Chen, X. H. Wang, J. Li, J. L. Lu and F. S. Wang, *Corrosion Science*, 2007, **49**, 3052-3063.
3. R. Arefinia, A. Shojaei, H. Shariatpanahi and J. Neshati, *Progress in Organic Coatings*, 2012, **75**, 502-508.
4. A. G. MacDiarmid, *Synthetic Metals*, 2001, **125**, 11-22.
5. S. Bhadra, D. Khastgir, N. K. Singha and J. H. Lee, *Progress in Polymer Science*, 2009, **34**, 783-810.
6. H. D. Tran and R. B. Kaner, *Chemical Communications*, 2006, 3915-3917.
7. U. Riaz, R. Jahan, S. Ahmad and S. M. Ashraf, *Journal of Applied Polymer Science*, 2008, **108**, 2604-2610.
8. P. A. Kilmartin, L. Trier and G. A. Wright, *Synthetic Metals*, 2002, **131**, 99-109.
9. T. D. Nguyen, T. A. Nguyen, M. C. Pham, B. Piro, B. Normand and H. Takenouti, *Journal of Electroanalytical Chemistry*, 2004, **572**, 225-234.
10. R. Jadhav, D. Hundiware and P. Mahulikar, *Journal of Coatings Technology and Research*, 2010, **7**, 449-454.
11. S. Chaudhari and P. P. Patil, *Electrochimica Acta*, 2007, **53**, 927-933.
12. B. Yao, G. Wang, X. Li and Z. Zhang, *Journal of Applied Polymer Science*, 2009, **112**, 1988-1993.
13. P. Fu, H. Li, J. Sun, Z. Yi and G.-c. Wang, *Progress in Organic Coatings*, 2013, **76**, 589-595.
14. F. Chen and P. Liu, *ACS Applied Materials & Interfaces*, 2011, **3**, 2694-2702.
15. M. Mobin and N. Tanveer, *Journal of Coatings Technology and Research*, 2012, **9**, 27-38.
16. N. Tanveer and M. Mobin, *Journal of Minerals and Materials Characterization and Engineering*, 2011, **10**, 735.
17. P. Fu, H. Li, J. Sun, Z. Yi and G.-c. Wang, *Progress in Organic Coatings*, 2013, **76**, 589-595.
18. S. Pathan and S. Ahmad, *Journal of Materials Chemistry A*, 2013, **1**, 14227-14238.
19. Y. Liu, D. Sun, H. You and J. S. Chung, *Applied Surface Science*, 2005, **246**, 82-89.
20. P. Muthirulan and N. Rajendran, *Surface and Coatings Technology*, 2012, **206**, 2072-2078.
21. M. Kashif and S. Ahmad, *RSC Advances*, 2014, **4**, 20984-20999.
22. S. Ahmad, U. Riaz, M. Kashif and M. Khan, *Journal of Inorganic and Organometallic Polymers and Materials*, 2012, **22**, 662-670.

23. E. P. Koval'chuk, N. V. Stratan, O. V. Reshetnyak, J. Błażejowski and M. S. Whittingham, *Solid State Ionics*, 2001, **141–142**, 217-224.
24. T. Siva, K. Kamaraj, V. Karpakam and S. Sathiyarayanan, *Progress in Organic Coatings*, 2013, **76**, 581-588.
25. A. C. C. de Leon, R. B. Pernites and R. C. Advincula, *ACS Applied Materials & Interfaces*, 2012, **4**, 3169-3176.
26. O. u. Rahman, S. C. Mohapatra and S. Ahmad, *Materials Chemistry and Physics*, 2012, **132**, 196-202.
27. Y. Jafari, M. Shabani-Nooshabadi and S. M. Ghoreishi, *Polymers for Advanced Technologies*, 2014, **25**, 279-287.
28. S. J. Lee, J. M. Lee, I. W. Cheong, H. Lee and J. H. Kim, *Journal of Polymer Science Part A: Polymer Chemistry*, 2008, **46**, 2097-2107.
29. B.-J. Kim, S.-G. Oh, M.-G. Han and S.-S. Im, *Synthetic Metals*, 2001, **122**, 297-304.
30. W.-S. Huang, B. D. Humphrey and A. G. MacDiarmid, *Journal of the Chemical Society, Faraday Transactions 1: Physical Chemistry in Condensed Phases*, 1986, **82**, 2385-2400.
31. S. Palraj, M. Selvaraj, M. Vidhya and G. Rajagopal, *Progress in Organic Coatings*, 2012, **75**, 356-363.
32. N. K. Rawat, A. Ghosal and S. Ahmad, *RSC Advances*, 2014, **4**, 50594-50605.
33. A. K. Dewan, D. P. Valenzuela, S. T. Dubey and A. K. Dewan, *Industrial & Engineering Chemistry Research*, 2002, **41**, 914-921.
34. M. Wang, H. Zhang, C. Wang, X. Hu and G. Wang, *Electrochimica Acta*, 2013, **91**, 144-151.
35. N. Pirhady Tavandashti, S. Sanjabi and T. Shahrabi, *Progress in Organic Coatings*, 2009, **65**, 182-186.
36. H. Wei, D. Ding, S. Wei and Z. Guo, *Journal of Materials Chemistry A*, 2013, **1**, 10805-10813.
37. S. V. Lamaka, M. F. Montemor, A. F. Galio, M. L. Zheludkevich, C. Trindade, L. F. Dick and M. G. S. Ferreira, *Electrochimica Acta*, 2008, **53**, 4773-4783.
38. H. Zhang, J. Wang, X. Liu, Z. Wang and S. Wang, *Industrial & Engineering Chemistry Research*, 2013, **52**, 10172-10180.
39. S. V. Lamaka, M. L. Zheludkevich, K. A. Yasakau, R. Serra, S. K. Poznyak and M. G. S. Ferreira, *Progress in Organic Coatings*, 2007, **58**, 127-135.
40. İ. Çakmakçı, B. Duran and G. Bereket, *Progress in Organic Coatings*, 2013, **76**, 70-77.
41. T. P. Chou, C. Chandrasekaran, S. J. Limmer, S. Seraji, Y. Wu, M. J. Forbess, C. Nguyen and G. Z. Cao, *Journal of Non-Crystalline Solids*, 2001, **290**, 153-162.
42. J. Fu, T. Chen, M. Wang, N. Yang, S. Li, Y. Wang and X. Liu, *ACS Nano*, 2013, **7**, 11397-11408.
43. M. Wang, M. Liu and J. Fu, *Journal of Materials Chemistry A*, 2015, **3**, 6423-6431.
44. J. N. Murray, L. D. Stephenson and A. Kumar, *Progress in Organic Coatings*, 2003, **47**, 136-146.
45. A. Kumar, L. D. Stephenson and J. N. Murray, *Progress in Organic Coatings*, 2006, **55**, 244-253.
46. P. J. Kinlen, D. C. Silverman and C. R. Jeffreys, *Synthetic Metals*, 1997, **85**, 1327-1332.

Caption to Illustration

Fig.1(a) Scheme for the formulation of P(oA-co-o-PDA) copolymer nanorods and nanocomposites

Fig. 1(b) Scheme for the formulation of DGEBA epoxy-polyamide (PA)

Fig.2(a-b) FT-IR spectra of epoxy matrix, P(oA-co-o-PDA) copolymer nanorods and

P(oA-co-o-PDA)-epoxy nanocomposite

Fig. 3 ^1H NMR of P(oA-co-o-PDA) nanorods

Fig.4 UV–Vis absorption spectra for P(oA-co-o-PDA) nanorods

Fig.5 (a) TEM micrograph of P(oA-co-o-PDA) nanorods

(b) SEM micrograph of P(oA-co-o-PDA) nanorods

(c) Enlarged view of SEM of single P(oA-co-o-PDA) nanorod

(d) SEM/EDAX of P (oA-co-o-PDA) nanorods

(e) TEM micrograph of PoA nanoparticles

(f) TEM micrographs of 3.0 % P (oA-co-o-PDA)-epoxy nanocomposite

Fig.6 XRD analysis of P(oA-co-o-PDA) nanorods

Fig.7 TGA of P(oA-co-o-PDA) nanorods

Fig.8 Contact angle images of neat epoxy, P(oA-co-o-PDA)-epoxy-PA and PoA-epoxy-PA nanocomposites

Fig. 9 Optical images of P(oA-co-o-PDA) copolymer coated CS (a) before cross hatch test (b) after cross hatch test (c) after EIS studies(5% NaCl)

Fig. 10 (a) Potentiodynamic polarization studies of uncoated and coated CS in 5.0 wt. % HCl

Fig. 10 (b) Potentiodynamic polarization studies of uncoated and coated CS in 5.0 wt. % NaCl

Fig. 11(a) Equivalent circuit model

Fig. 11(b-e) EIS studies of uncoated and coated CS in 5.0 wt. % HCl and 5.0 wt. % NaCl

Fig. 12(a) SEM-EDAX of Plain epoxy coating

Fig. 12 (b) SEM/EDAX of P(oA-co-o-PDA)-epoxy-PA nanocomposite coatings

Fig. 13 Raman spectra of epoxy-PA coated and P (oA-co-o-pda)-epoxy-PA coated CS after SST.

Table 1 Solubility test

Table 2 Physico-mechanical properties of epoxy, PoA-epoxy-PA and P(oA-co-oPDA)-epoxy-PA nano composite coatings

Table 3(a) Electrochemical parameters obtained from PDP and EIS studies for uncoated and coated CS in 5 % HCl at room temperature.

Table 3 (b) Electrochemical parameters obtained from PDP and EIS studies for uncoated and coated CS in 5% NaCl at room temperature.

Table 4 Raman bands assignments for nanocomposite coatings.

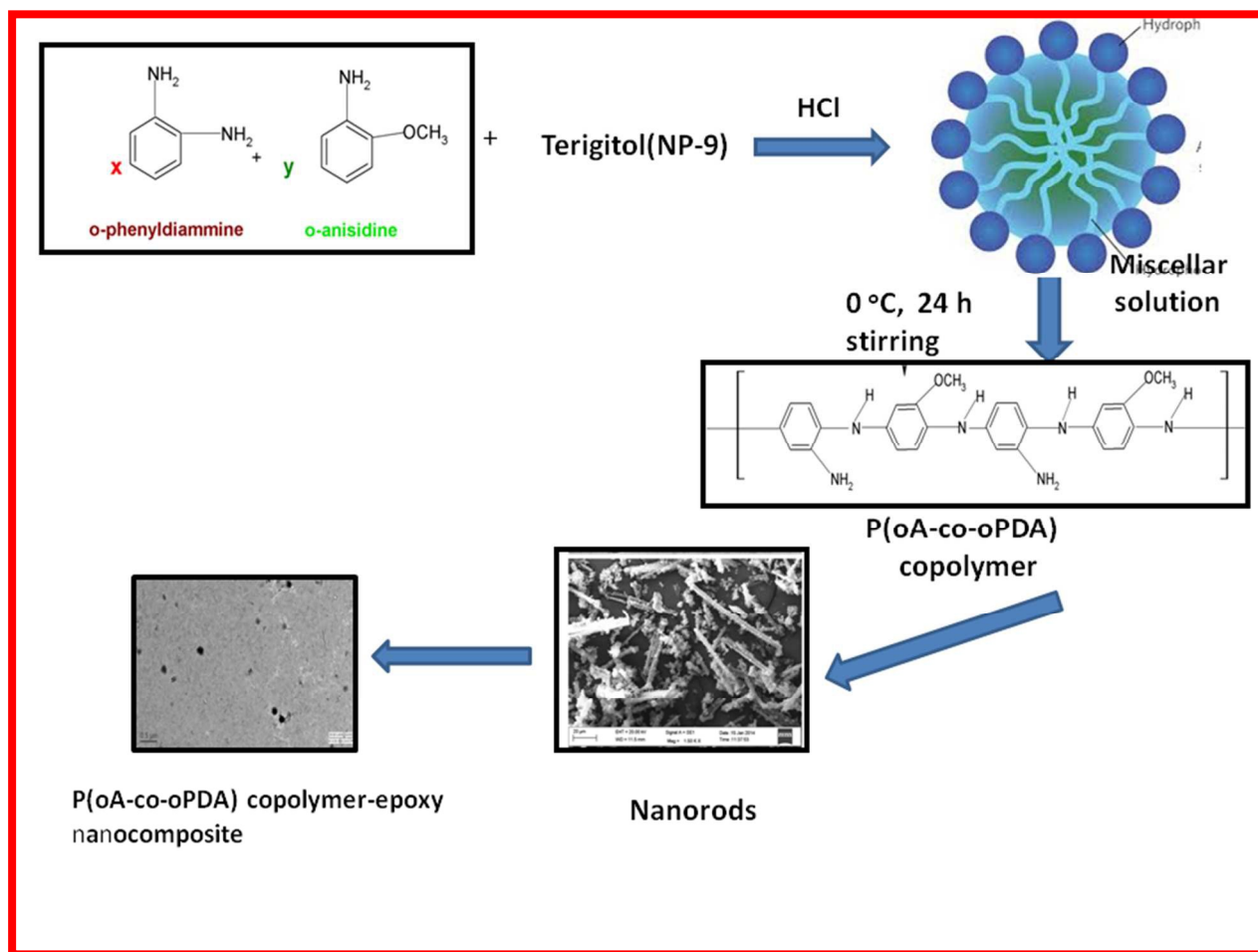


Fig.1(a) Scheme for the formulation of P(oA-co-o-PDA) copolymer nanoparticles

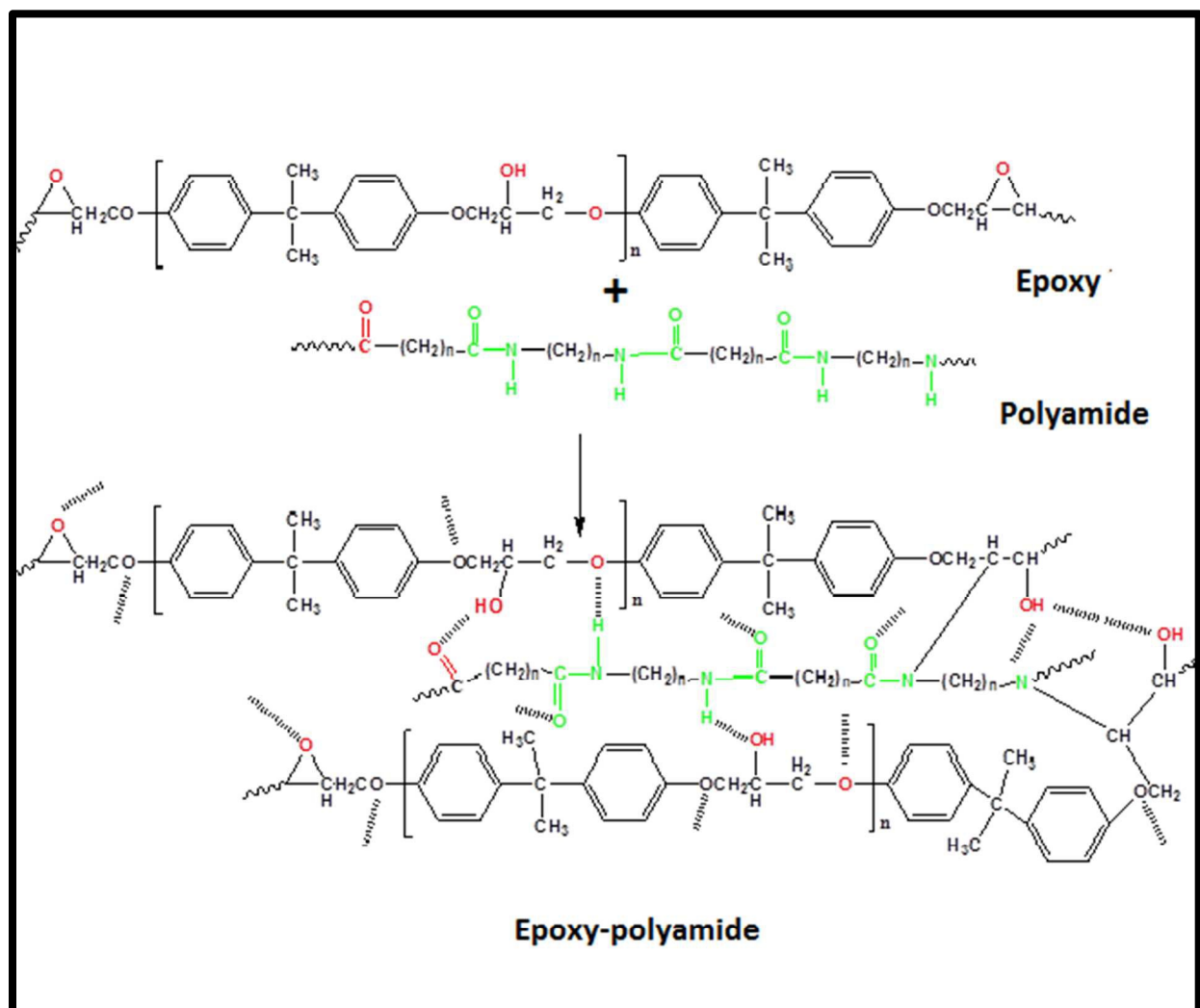


Fig. 1(b) Scheme for the formulation of DGEBA epoxy-polyamide (PA)

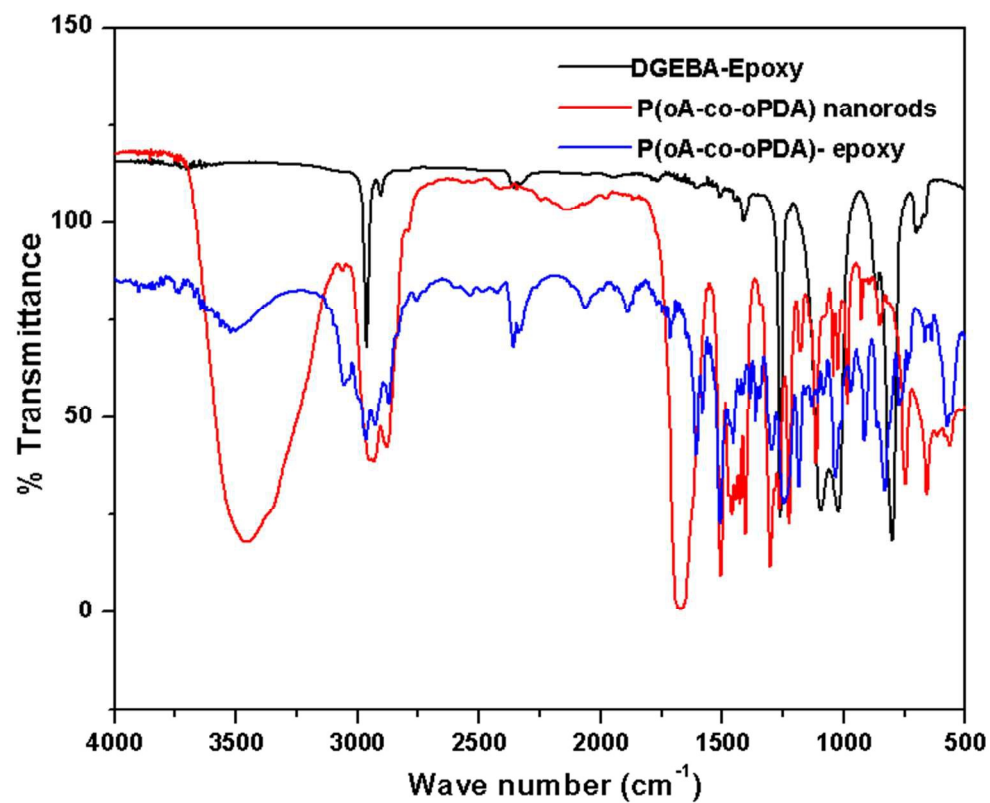


Fig. 2(a) FT-IR spectra of epoxy, P(oA-co-o-PDA)copolymer, and P(oA-co-o-pda-epoxy) nanocomposite.

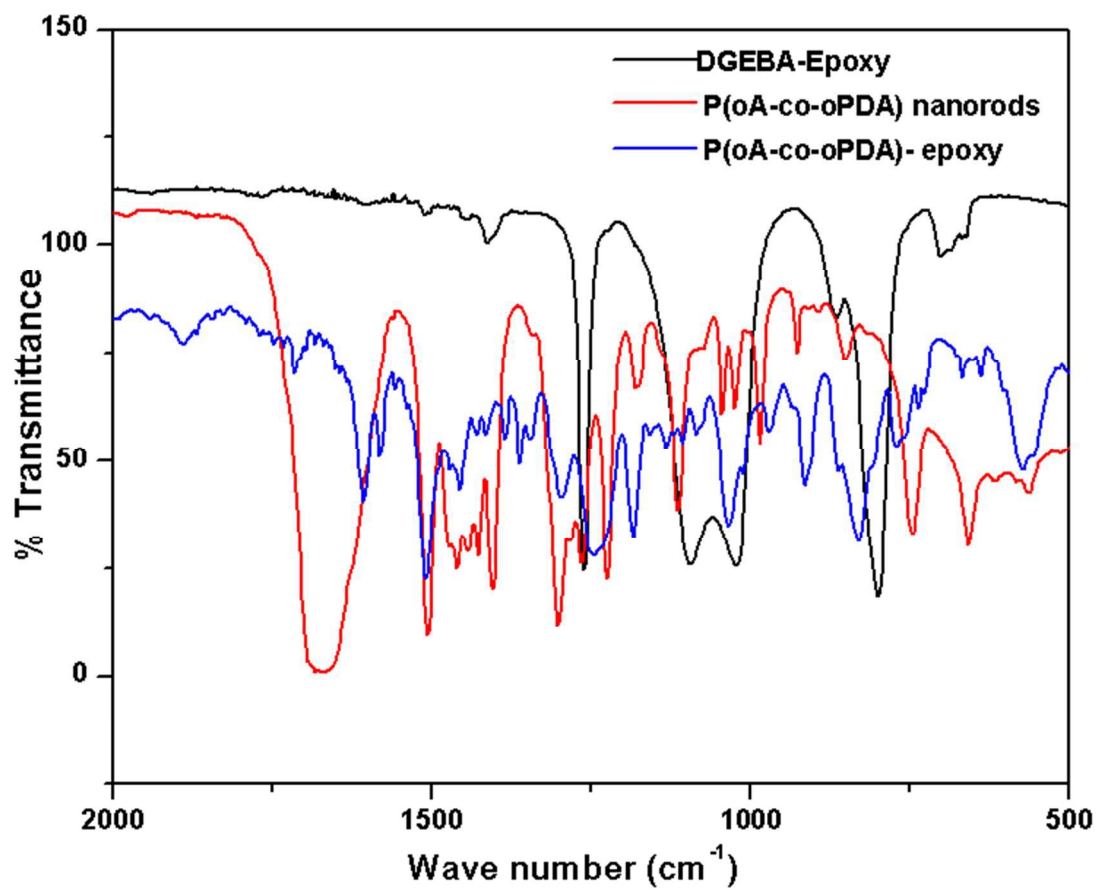


Fig.2 (b) FT-IR spectra of epoxy, P(oA-co-o-PDA) copolymer, and P(oA-co-o-pda-epoxy) nanocomposite in range 2000-500 cm⁻¹

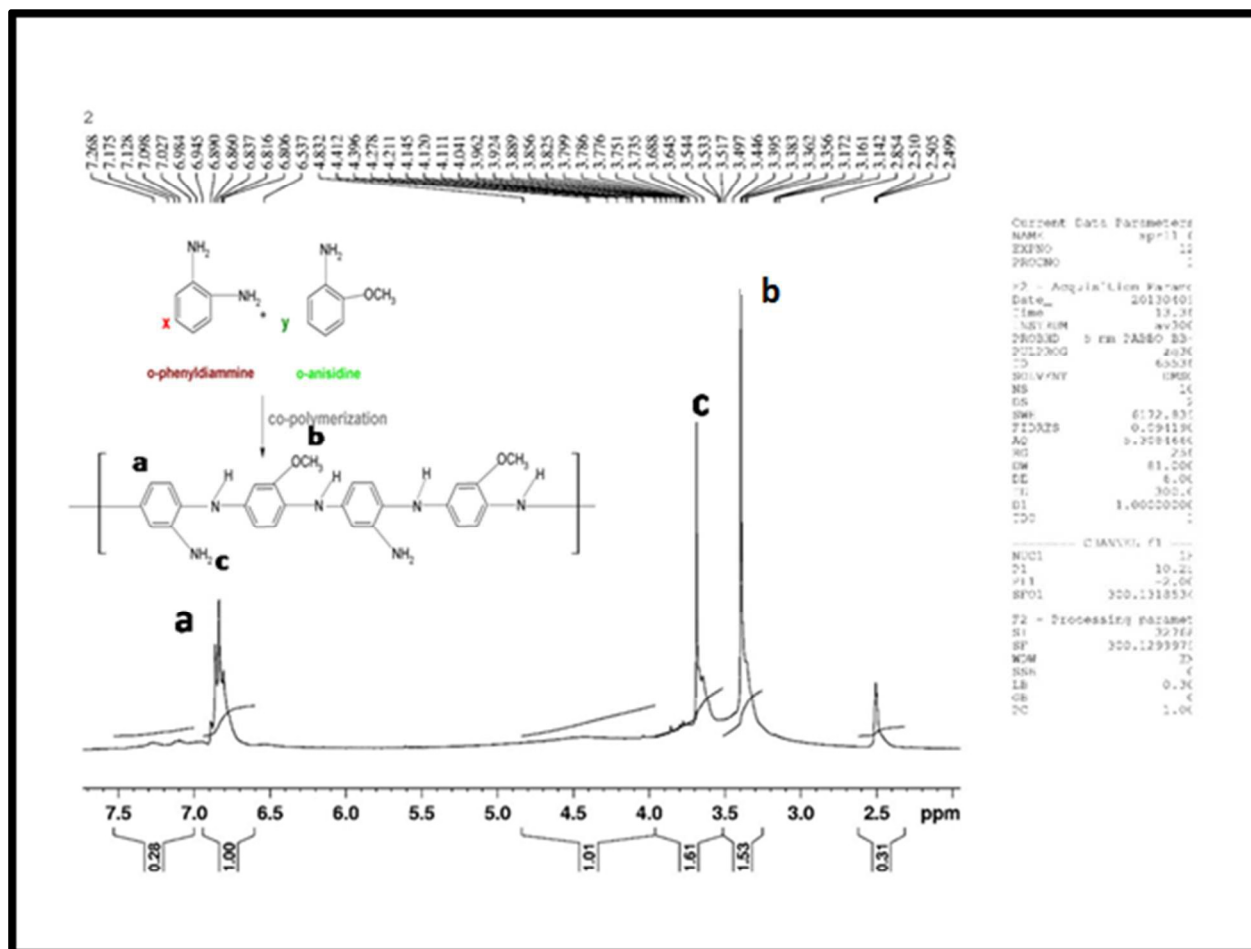


Fig. 3 ¹H NMR of P(oA-co-o-PDA) nanorods

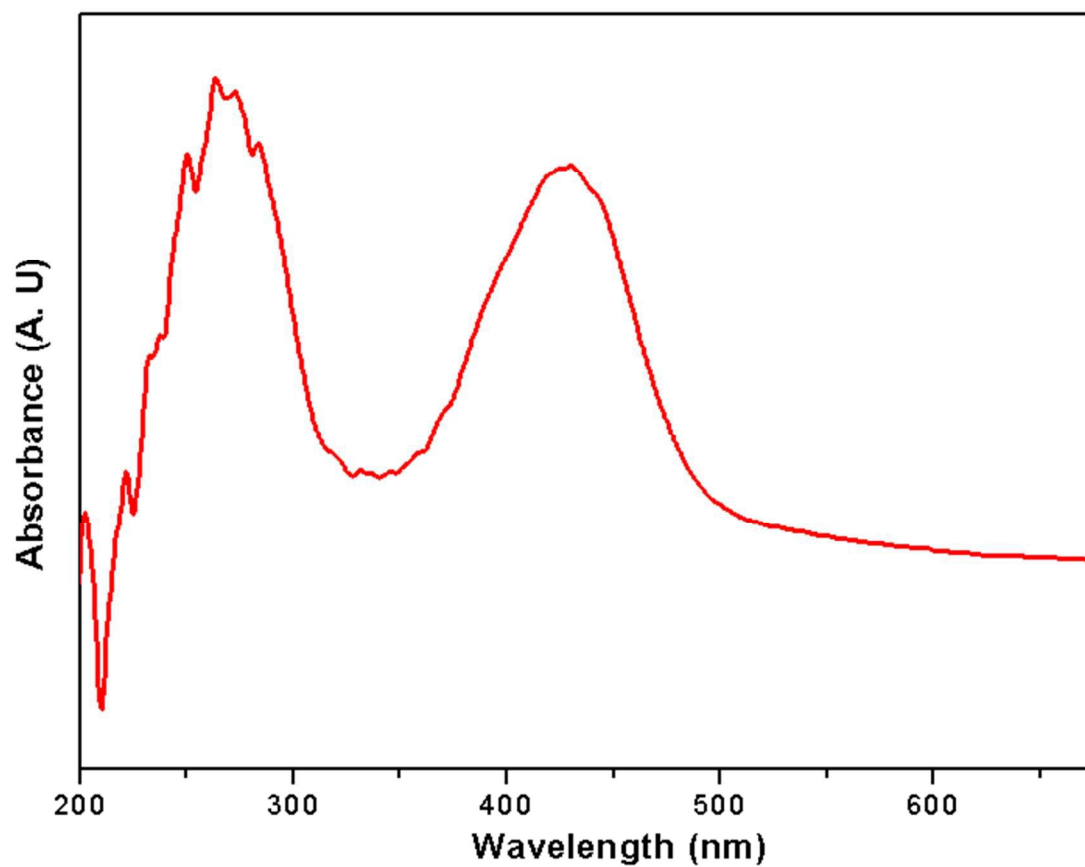


Fig. 4 UV–Vis absorption spectra for P(oA-co-o-PDA) nanorods

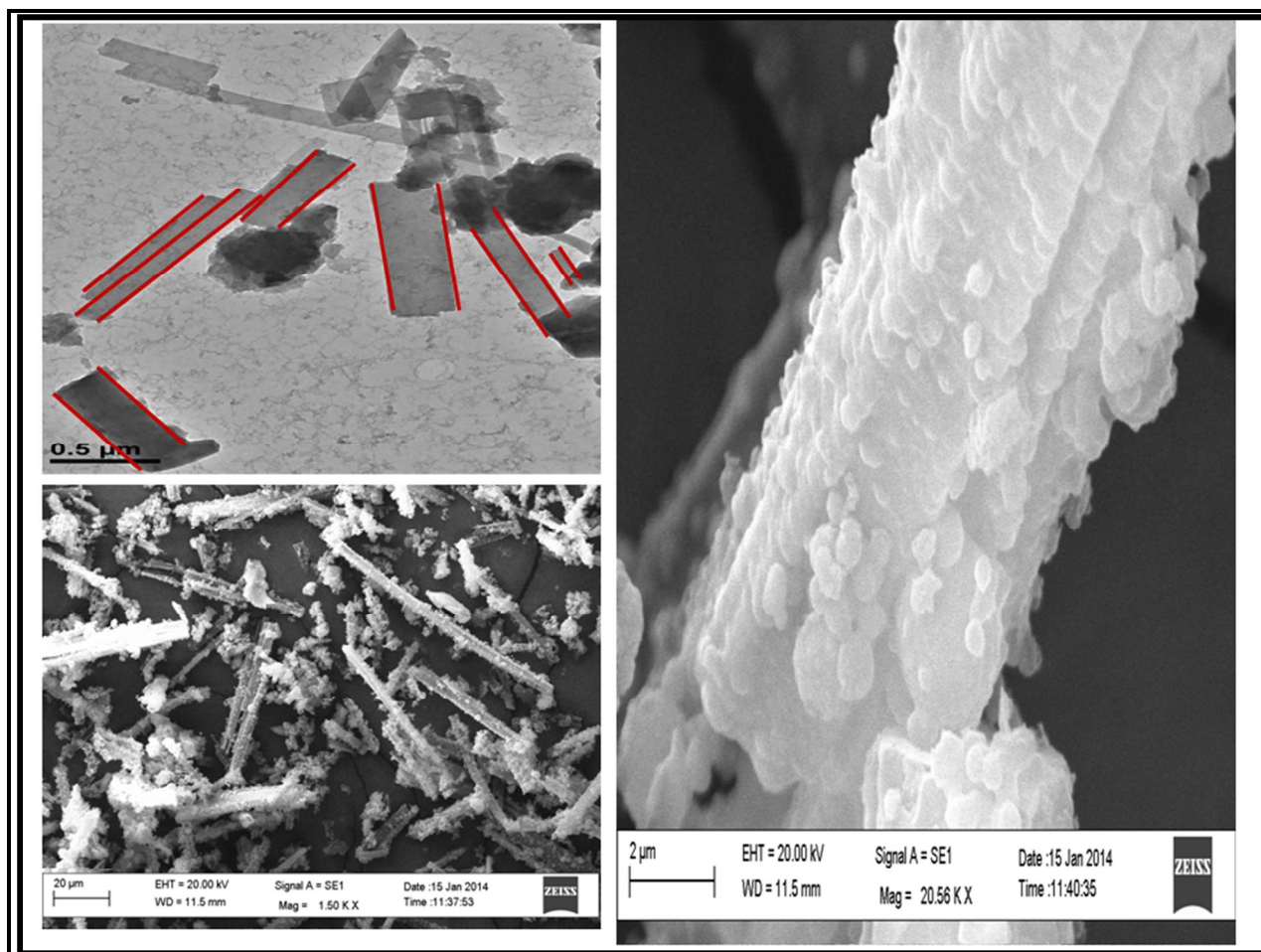


Fig 5(a) TEM and **(b)** SEM analysis for P(oA-co-o-PDA) nanorods **(c)** Enlarged view of SEM of single P(oA-co-o-PDA) nanorod

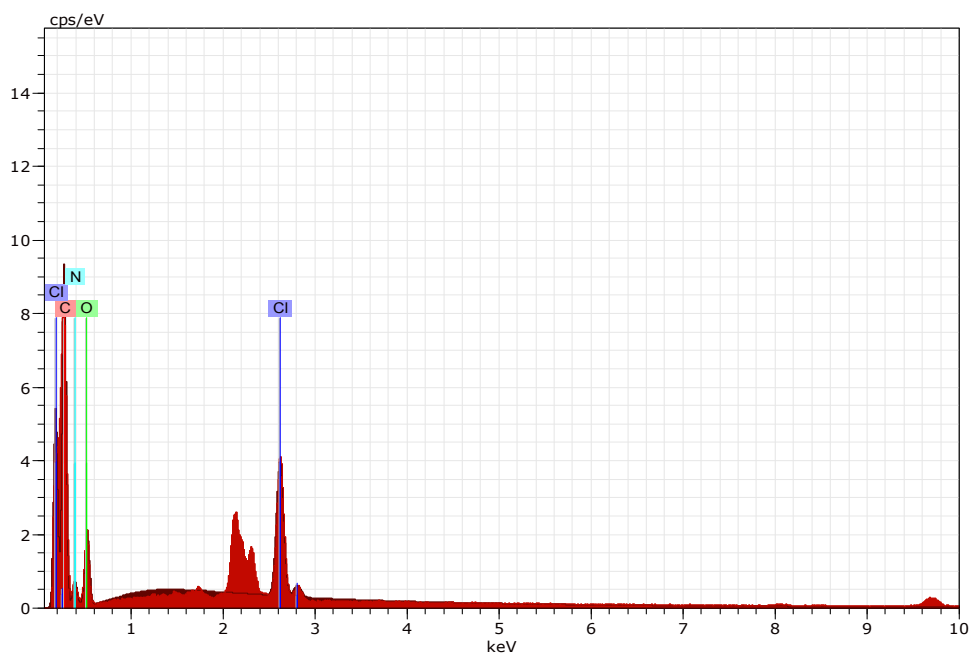


Fig.5 (d) SEM/EDAX of P (oA-co-o-PDA) nanorods

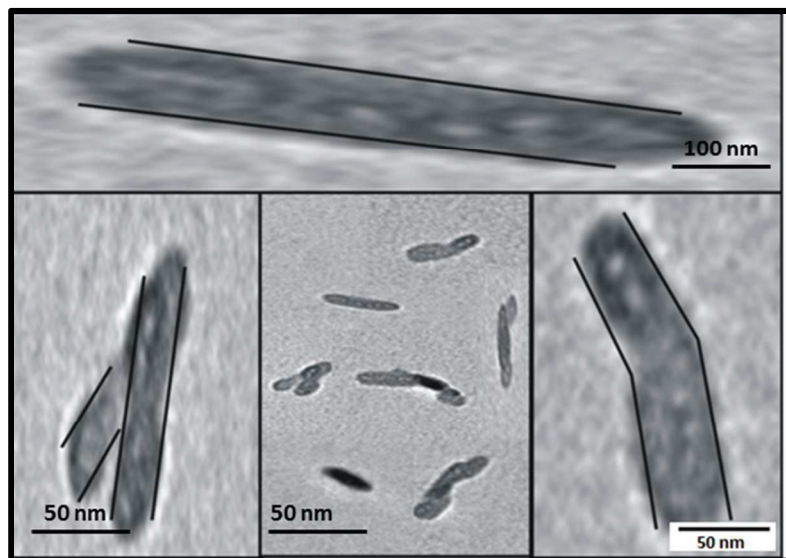


Fig. 5(e) TEM micrograph of PoA nanoparticles (centre) and enlarged view of PoA (left, right and above)

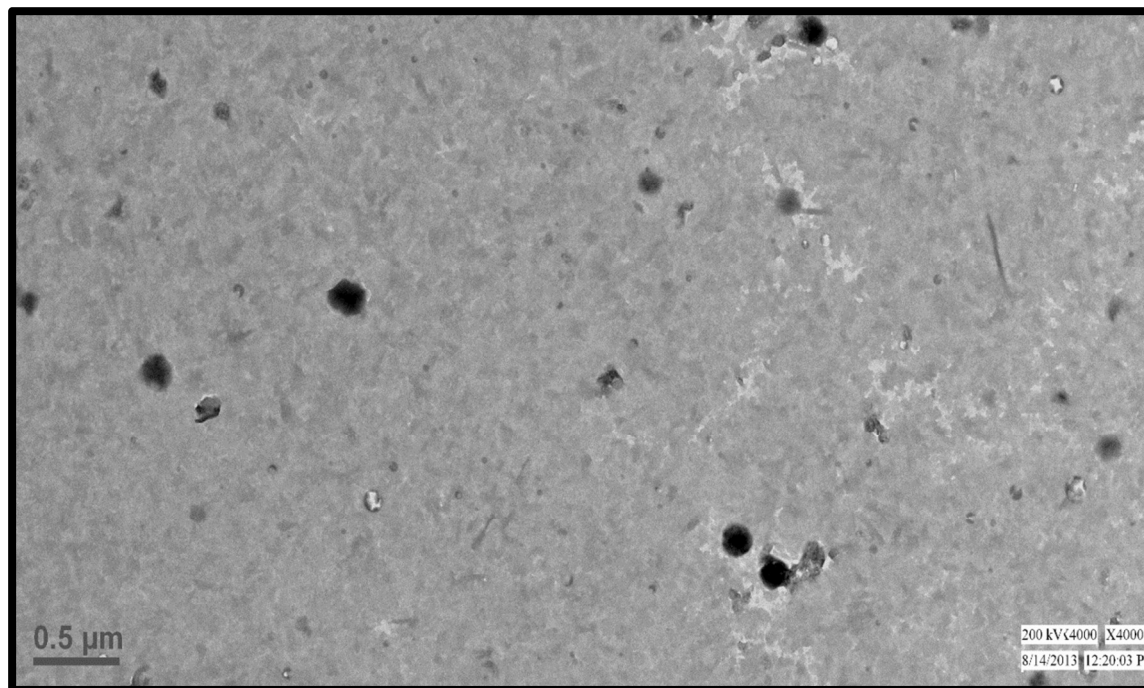


Fig. 5 (f) TEM micrographs of 3.0 % P(oA-co-o-PDA) -epoxy nanocomposite

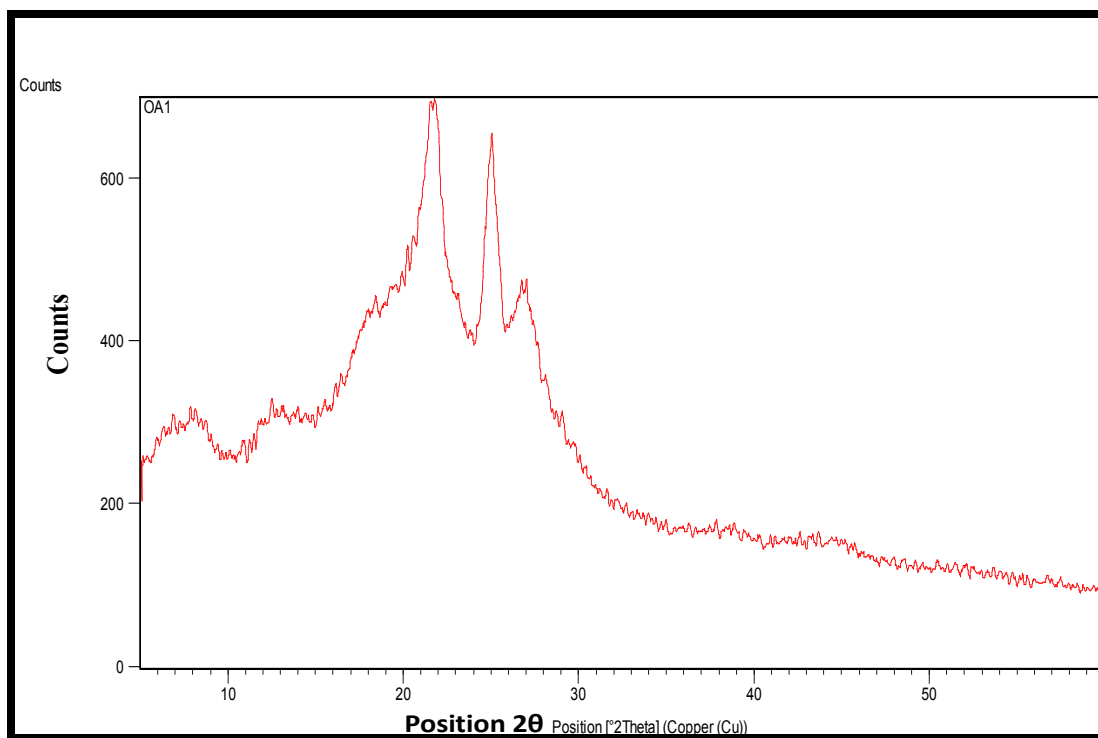


Fig. 6 XRD analysis of P(oA-co-o-PDA) nanorods

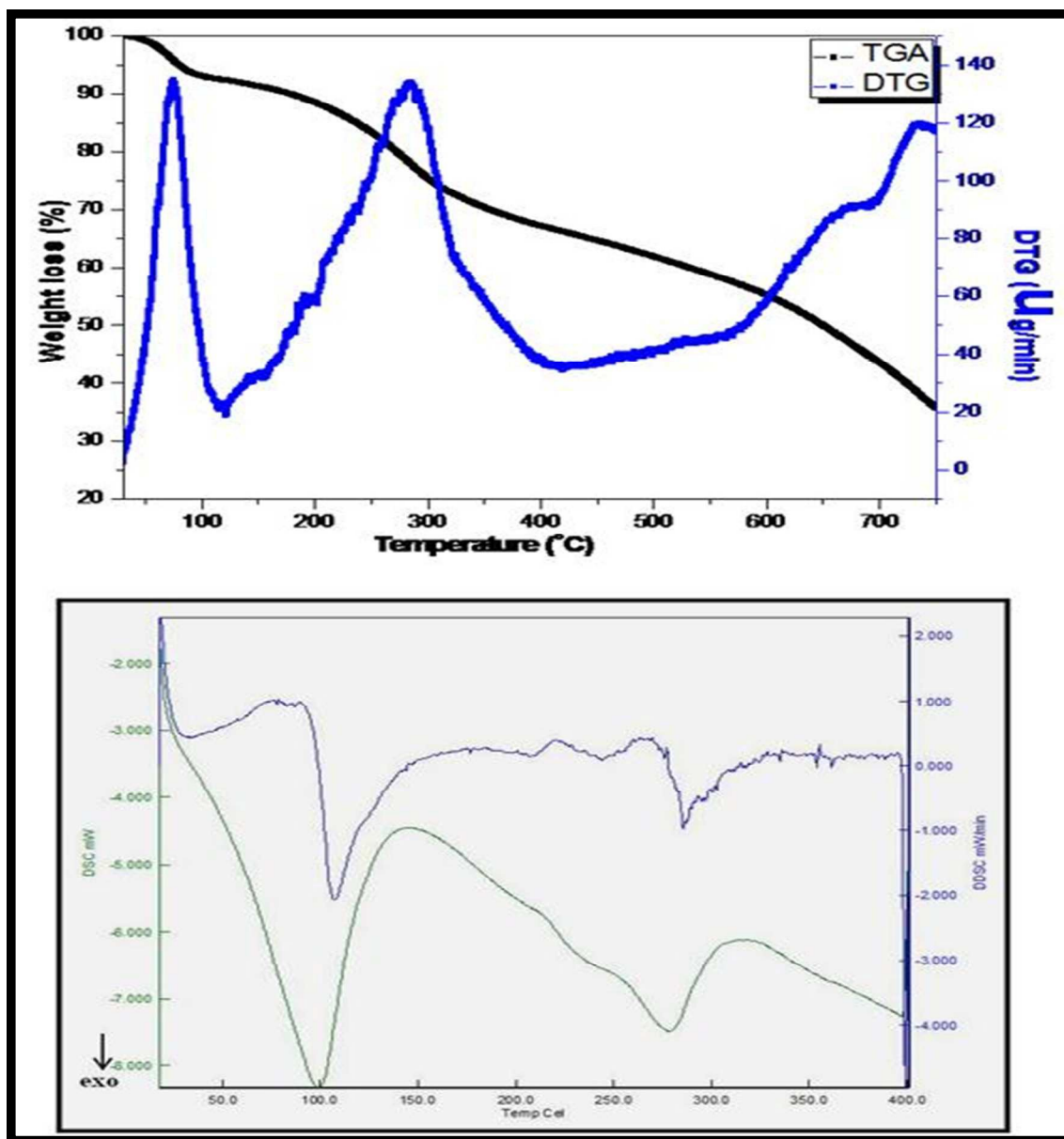


Fig. 7 TGA and DSC of P (oA-co-o-PDA) nanorods

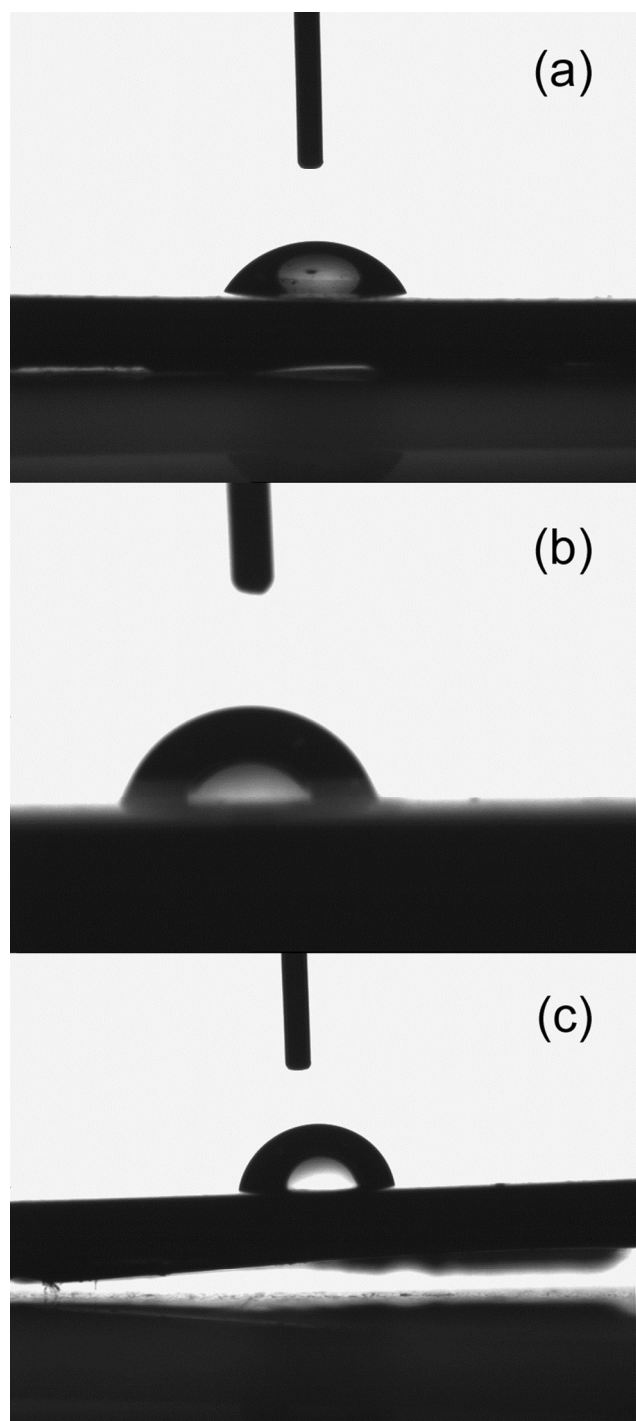


Fig. 8 Contact angle images (a) epoxy plain (b) PoA-epoxy-PA (c) P(OA-co-opda)-epoxy-PA

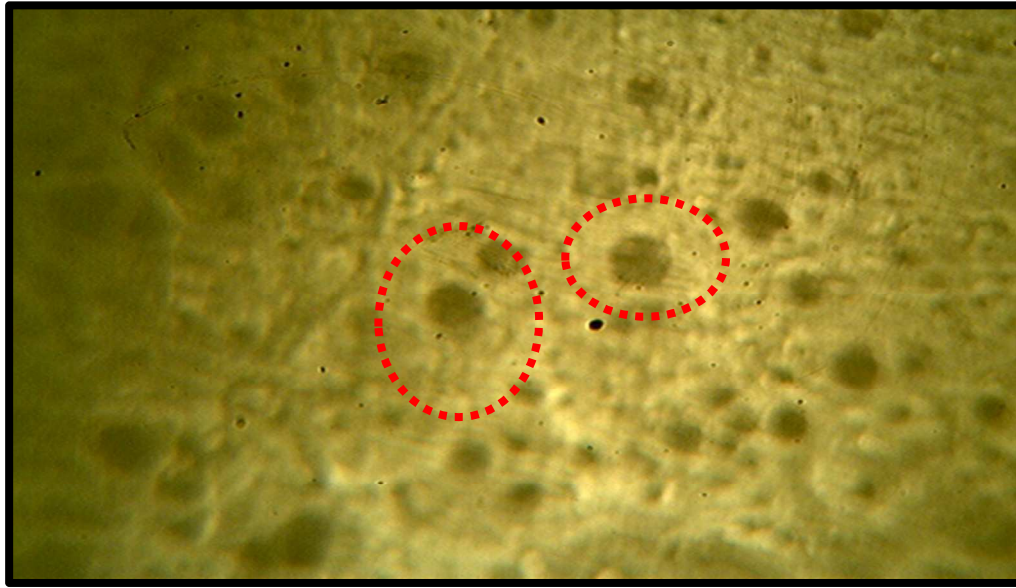


Fig. 9(a) Optical images of PoA-co-opda)-epoxy-PA coated CS

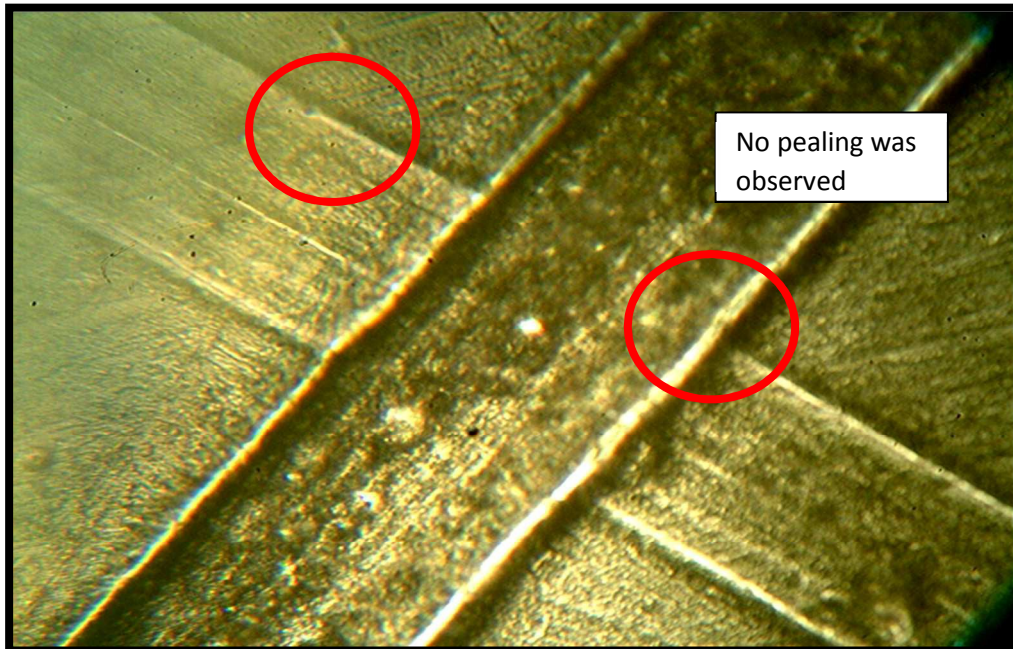


Fig.9(b) Optical images of P(oA-co-opda)-epoxy-PA coated CS after cross hatch test



Fig. 9 (c) Optical images of P(oA-co-opda)-epoxy-PA coated CS after EIS studies

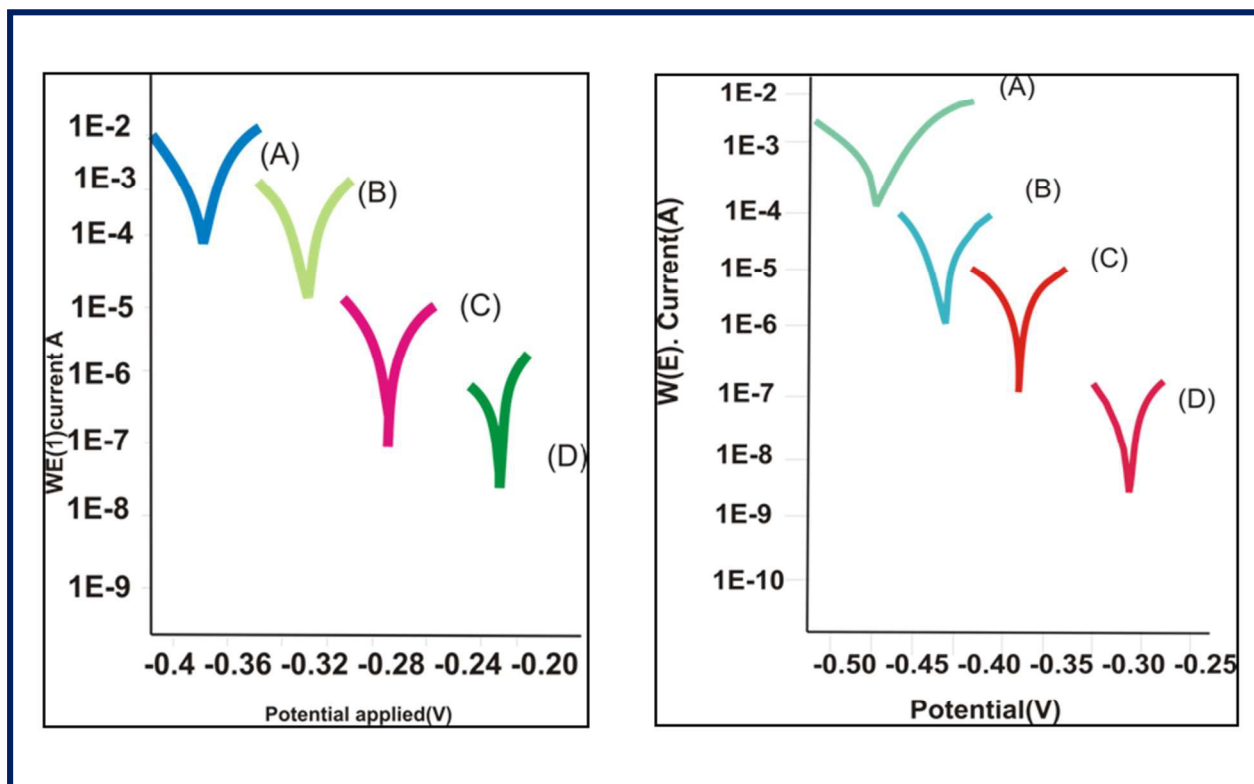


Fig. 10 (a) PDP curves of (A) CS (B) Epoxy(C) POA-epoxy-PA (D) P(oA-co-oPDA)-epoxy-PA coated CS in 5 % HCl

Fig. 10 (b) PDP curves of (A) CS, (B) Epoxy (C) POA-epoxy- PA (D)P(oA-co-opda)-epoxy-PA coated CS in 5 % NaCl

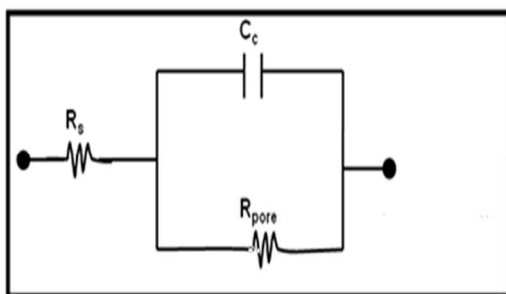


Fig 11(a) Fitted EIS circuit

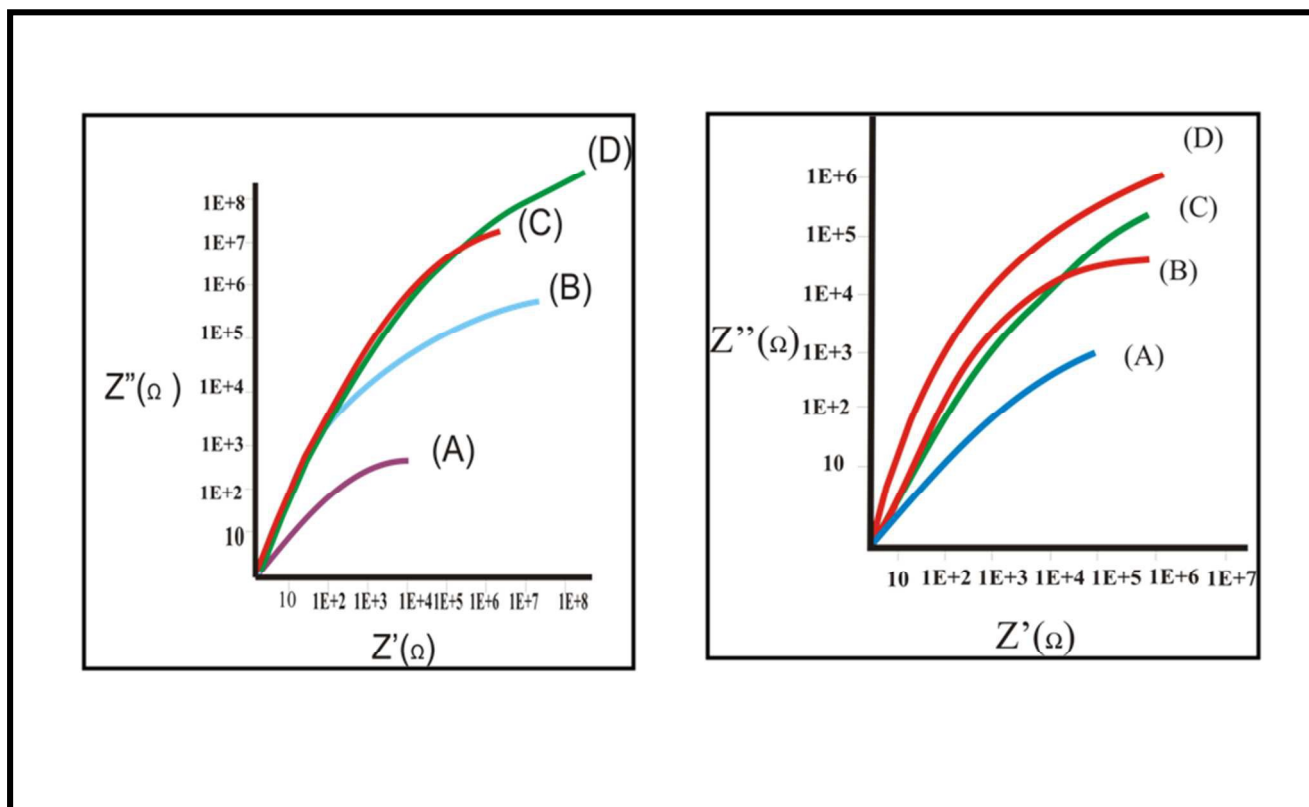


Fig. 11(b) EIS spectra of (Nyquist plots) (A) CS, (B) epoxy (C) PoA-epoxy, (D) P(oA-co-oPDA) epoxy-PA coated CS in 5 % HCl

Fig. 11(c) EIS spectra of (Nyquist plots) (A) CS, (B) epoxy (C) POA-epoxy, (D) P(OA-co-oPDA) epoxy-PA coated CS in 5 % NaCl

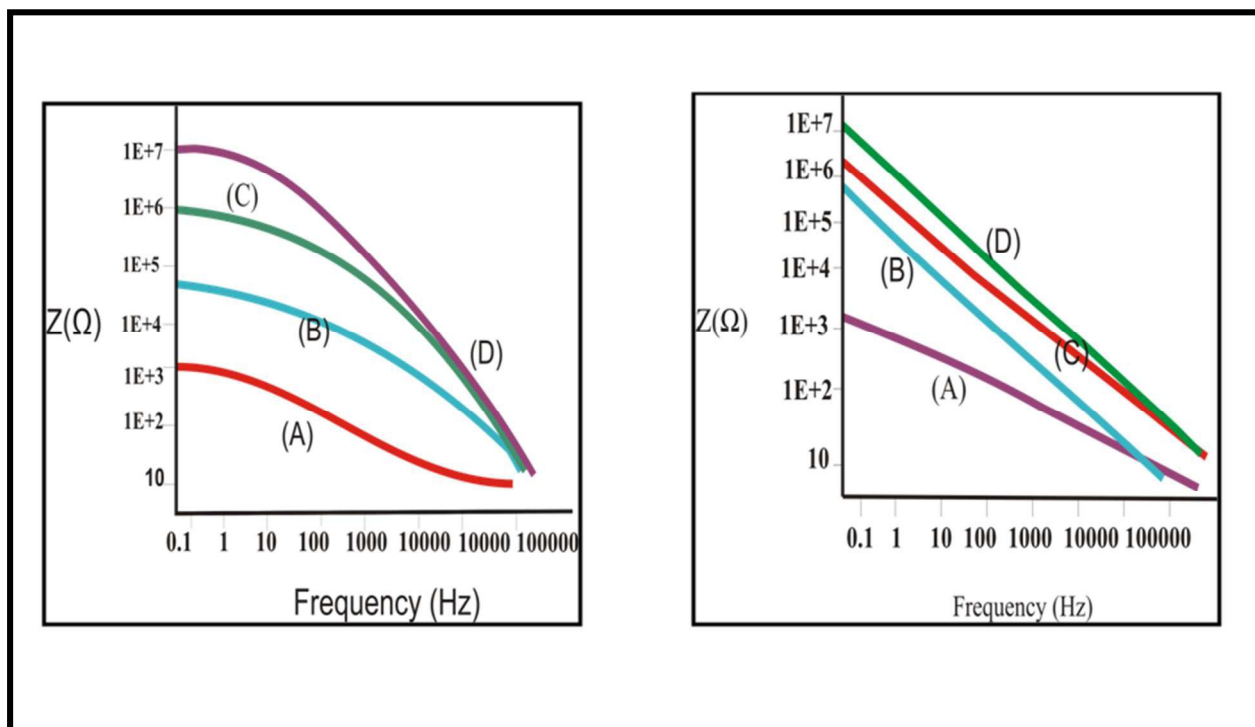


Fig. 11(d) EIS spectra of (Bode plots) (A) CS, (B) epoxy (C) PoA-epoxy-PA (D) P(oA-co-oPDA)- epoxy-PA coated CS in 5 % NaCl

Fig. 11(e) EIS spectra of (Bode plots) (A) CS, (B) epoxy (C) PoA-epoxy, (D) P(oA-co-oPDA)- epoxy-PA coated CS in 5 % HCl



Fig. 12(a) SEM of neat epoxy

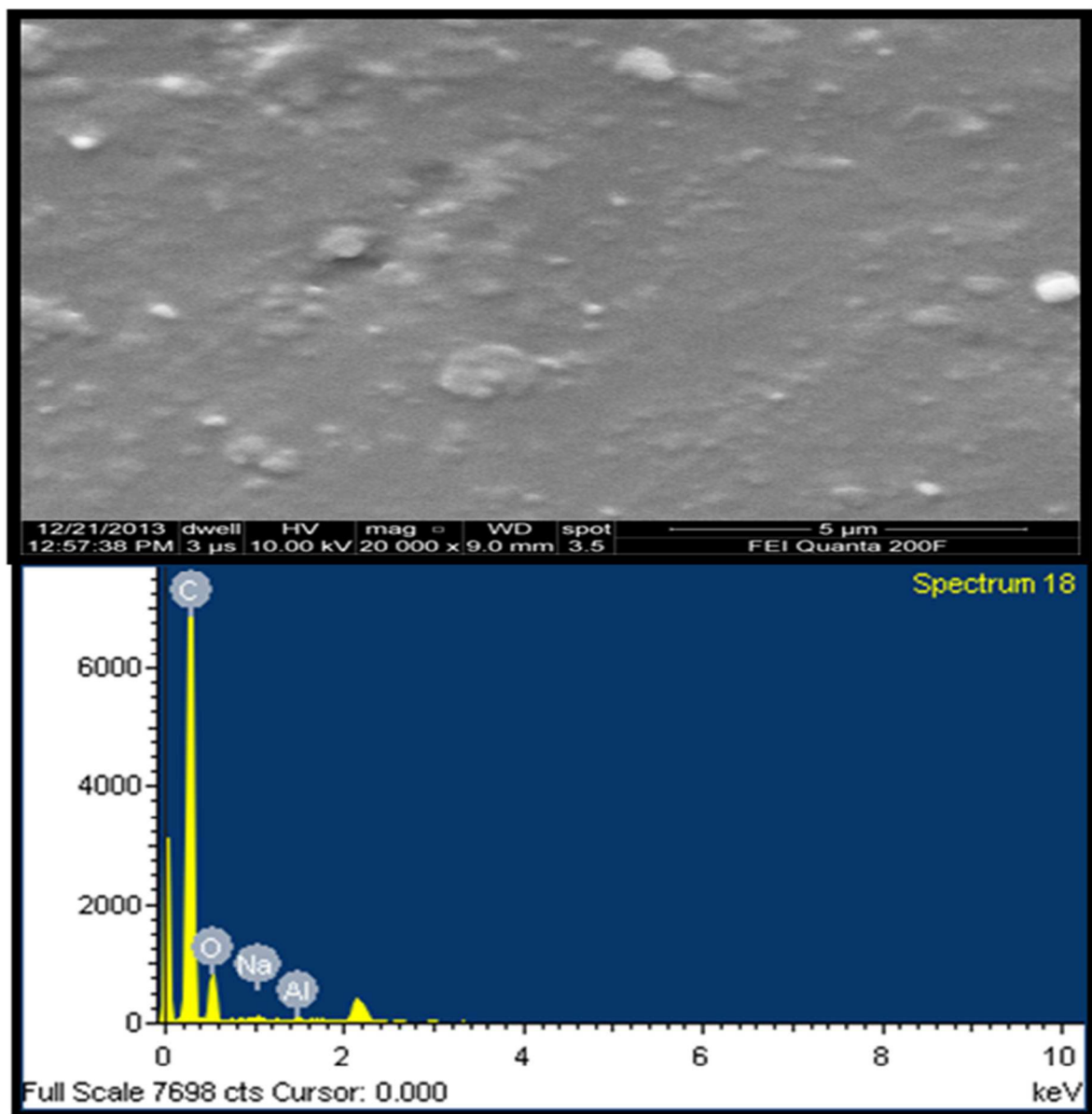


Fig.12(b) SEM micrograph of P(oA-co-o-PDA)-epoxy-PA coated CS and EDAX spectra of P(oA-co-o-PDA)-epoxy-PA coated CS

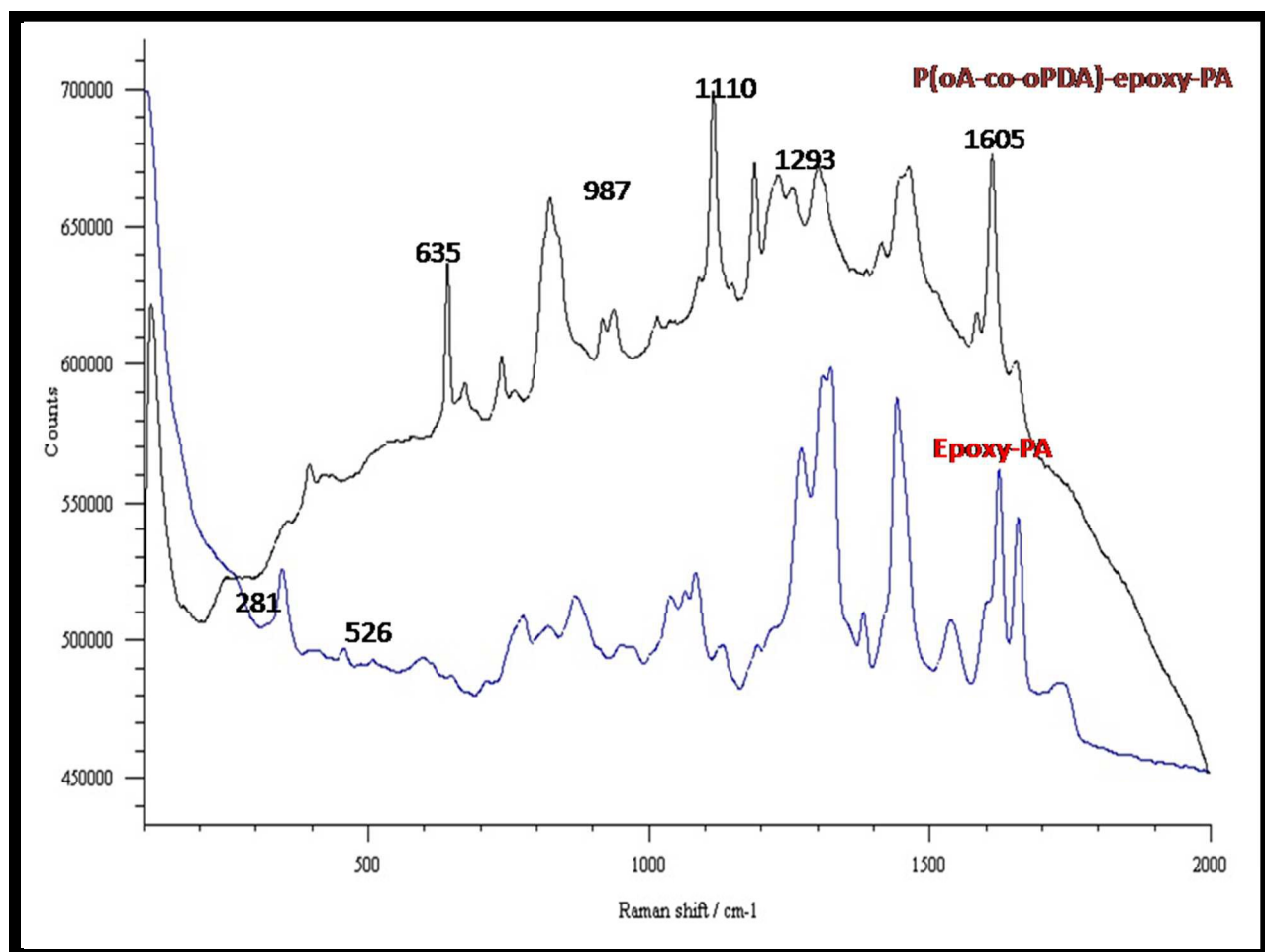


Fig. 13. Raman spectra of epoxy coated and P (oA-co-o-pda)-epoxy-PA coated CS

Table 1. Solubility test

Solvents	Solubility		
	Epoxy	PoA	P(oa-co-opda) copolymer
Xylene	Insoluble	Insoluble	Insoluble
DMF	Soluble	Soluble	Soluble
DMSO	Partly soluble	Soluble	Soluble
Toluene	Insoluble	Partially soluble	Insoluble
CCl₄	Insoluble	Insoluble	Insoluble
THF	Insoluble	Insoluble	Insoluble
Acetone	Partially soluble	Partially soluble	Partially soluble
Benzene	Insoluble	Insoluble	Insoluble
Ethylmethyl ketone	Soluble	Soluble	Soluble
Ethanol	Insoluble	Soluble	Partially soluble
Methanol	Soluble	Soluble	Soluble
NMP	Insoluble	Soluble	Partially Soluble

Table 2. Physico-mechanical properties of epoxy, PoA-epoxy-PA and PoA-co-opda-epoxy-PA nano composite coatings

Test	Epoxy	PoA-epoxy-PA	PoA-co-opda-epoxy-PA
Scratch Hardness	6.5 Kg	11.2 Kg	12.9 Kg

Impact resistance	150lb/inch	150lb/inch	150lb/inch
Gloss at45°	38	35	33
Bending 1/8inch	Pass	Pass	Pass
Cross hatch test	Pass	Pass	Pass

Table 3(a). Electrochemical parameters obtained from PDP and EIS studies for uncoated and coated CS in 5 % HCl at room temperature.

Sample	Ecorr (V)	Icorr (A cm ⁻²)	Rp (Ω)	Rpore (Ω)	Cc(farad)
CS	-0.33285	5.5197E-4	33.469	2.4x10 ³	7.1x10 ⁻⁵
Epoxy	-0.28424	2.6594E-5	967.07	6.1x10 ³	2.9x10 ⁻⁷
PoA-epoxy-PA	-0.28899	2.1884E-6	3228.3	2.3x10 ⁵	3.6x10 ⁻⁹
P(oA-co-o-PDA) –epoxy-PA	-0.22403	1.3666E-7	1799.1	3.1x10 ⁷	7.8x10 ⁻¹⁰

Table 3(b). Electrochemical parameters obtained from PDP and EIS studies for uncoated and coated CS in 5% NaCl at room temperature.

Sample	Ecorr (V)	Icorr (a cm ⁻²)	Rp (Ω)	Rpore (Ω)	Cc(farad)
CS	-0.24017	7.9416E-4	7032.2	1.2x10 ³	1.8x10 ⁻³
Epoxy-PA	-0.26254	5.9084E-6	39272	2.2x10 ⁴	2.32x10 ⁻⁴
PoA-epoxy-PA	-0.38021	2.4207E-7	29121	1.27x10 ⁶	9.67x10 ⁻⁶
P(oA-co-o-PDA) –epoxy-PA	-0.40885	4.3782E-8	7751.1	1.72x10 ⁷	7.9x10 ⁻¹⁰

Table 4. Raman bands assignments for nanocomposite coatings.

Band position (cm ⁻¹)	Assignments
1605	C - C stretching vibration of aromatic; C - O stretching vibration of amide; skeletal vibrations of C- C double bonds in aromatic ring
1220	C - O stretching vibration ether bridge C - O stretching vibration of secondary alcohol
987	Epoxy group
657	Aromatic ring vibrations (o-substituted benzene); aromatic C- H out of plane deformation
216, 281 and 1293	are assigned to Fe ₂ O ₃ showing the formation of a passive layer